# MAJORANA FERMIONS AND PARAFERMIONS IN HYBRID SUPERCONDUCTOR/SEMICONDUCTOR SYSTEMS

A Dissertation

Submitted to the Faculty

of

Purdue University

by

Jingcheng Liang

In Partial Fulfillment of the

Requirements for the Degree

of

Doctor of Philosophy

December 2018

Purdue University

West Lafayette, Indiana

# THE PURDUE UNIVERSITY GRADUATE SCHOOL
# STATEMENT OF DISSERTATION APPROVAL

Dr. Yuli Lyanda-Geller, Chair

Department of physics and Astronomy

Dr. Gabor Csathy

Department of physics and Astronomy

Dr. Martin Kruczenski

Department of physics and Astronomy

Dr. Leonid Rokhinson

Department of physics and Astronomy

**Approved by:**

Dr. John Finley

Head of the School Graduate Program

For my parents.

# ACKNOWLEDGMENTS

I would like to express my special appreciation and gratitude to my advisor, Prof. Lyanda-Geller for his education and guidance. I feel grateful for all his help, advice and encouragement in my research. I also want to thank Prof. Csathy, Prof. Kruczenski and Prof. Rokhinson for serving as my thesis committee members and Prof. Hu as my prelim committee member. Special thanks to Prof. Kruczenski for helpful guidance of quantum field theory.

I would also like to thank my parents. They help me recognize the beauty of the knowledge. Without their support, I will not be able to enter the graduate school to pursue the academic career.

I want to thank my friend George Simion, who helps me a lot in research. I also want to thank my friends Changchun Zhong, Qiang Zhang, Bin Yan, Marius Adrian Radu, Jie Hui, Kui Zhang for their help.

TABLE OF CONTENTS

# LIST OF FIGURES

Figure Page

Figure Page

Figure Page

# ABSTRACT

Liang, Jingcheng Ph.D., Purdue University, December 2018. Majorana Fermions and Parafermions in Hybrid Superconductor/Semiconductor Systems. Major Professor: Yuli Lyanda-Geller.

The quantum phase transitions and exotic excitations are exciting and important topics of nowadays condensed matter theory. Topologically protected excitations are of great interest for potential applications in quantum computing. This Thesis explores two examples of exotic topologically protected excitations, Majorana fermions and parafermions in hybrid superconductor/semiconductor systems.

In the first part of the thesis, after a brief review of ideas on Majorana zero modes in solid state systems obtained by researchers over the past decade, I present our study of the emergence of Majorana fermions in charge carrier holes doped quantum wires. Study of Majorana modes in this system requires understanding Luttinger holes in low dimensions, which is also crucial for numerous spin-dependent phenomena, emerging field of spintronics and nanotechnology. We find that hole-doped quantum wires that are proximity coupled to a conventional s-wave superconductor is a promising system for the observation of Majorana fermions. We advanced understanding of Luttinger holes in quantum wells and quantum wires. We have shown that the vast majority of earlier treatments of Luttinger holes ignored an important effect, a mutual transformation of heavy and light holes at the heteroboundaries. We have derived the effective hole Hamiltonians in the ground size-quantized sub-bands of quantum wells and quantum wires. The effect of mutual transformation of holes is crucial for understanding Zeeman and spin-orbit coupling, and results in several spin-orbit terms linear in momentum in hole-doped quantum wires. We discuss the criterion for realizing Majorana modes in charge carrier hole systems and show that GaAs or InSb hole wires shall exhibit stronger topological superconducting pairing, providing

additional opportunities for its control compared to intensively studies InSb and InAs electron systems.

In the second part of the thesis, I first introduce the basic facts of the current theoretical understanding of the fractional quantum Hall effect and a theoretical model of parafermion excitations. Parafermion zero modes are promising for universal quantum computing. However, physical systems that are predicted to host these exotic excitations are rare and difficult to realize in experiments. I present our work on modeling domain walls on the boundary between gate-induced polarized and unpolarized domains of the fractional quantum Hall effect system near the spin transitions, and the emergence of the parafermion zero modes when such domain wall is proximity coupled to an s-wave superconductor. Exact diagonalization of the Hamiltonian in a disk and torus geometries proves formation of the counter-propagating edge states with different spin polarizations at the boundaries between areas of the electron liquid in polarized and unpolarized filling factor $\nu = 2/3$ phases. By analytical and numerical methods we find the conditions for emergence of parafermion zero modes in hybrid fractional quantum Hall/s-wave superconductor system. The phase diagram indicates that the parafermionic phase, which is represented by the six-fold ground state degeneracy, is separated from other phases by a topological phase transition. Such parafermion modes are experimentally feasible. They present a vital step toward the realization of Fibonacci anyons that allow a full universal set of quantum operations with topologically protected quasiparticles.

# 1. INTRODUCTION TO MAJORANA FERMIONS

In this chapter I will give a brief introduction to Majorana fermions. I will first review the original version of Majorana fermions that comes from Majorana [1]. Then I will introduce Kitaev's model [2]. This model is exactly solvable and has Majorana fermions, or sometimes called Majorana zero modes in condensed matter context, as its low energy excitations. The 2D version of Kitaev's model is also discussed. Furthermore, I will discuss the non-Abelian exchange statistics which is implied in the constructions of Majorana zero modes and which makes Majorana zero modes so important for the realizations of topological quantum computation. In the last section, I will introduce one physical realization of Majorana zero modes in hybrid semiconductor/superconductor systems.

## 1.1 Overview of Majorana fermions

In 1928, Dirac discovered his brilliant equation that describes spin $\frac{1}{2}$ particles [3]:

$$(i\gamma^\mu \partial_\mu - m)\psi = 0 \tag{1.1}$$

where the field $\psi$ has four components and the $\gamma$ matrices are required to satisfy the Clifford algebra which is:

$$\{\gamma^\mu, \gamma^\nu\} = \gamma^\mu\gamma^\nu + \gamma^\nu\gamma^\mu = 2\eta^{\mu\nu} \tag{1.2}$$

where $\eta^{\mu\nu}$ is $diag(1, -1, -1, -1)$, the metric tensor for flat spacetime. In the chiral representation, the $\gamma$ matrices can be written explicitly [4]:

$$\gamma^0 = \begin{pmatrix} 0 & I_{2\times2} \\ I_{2\times2} & 0 \end{pmatrix} \quad , \quad \gamma^i = \begin{pmatrix} 0 & \sigma^i \\ -\sigma^i & 0 \end{pmatrix} \tag{1.3}$$

We observe that the elements of $\gamma$ matrices consist of both real and imaginary numbers, therefore the solution to Eq. (1.1) should be a complex field. In quantum field theory, if the field $\psi$ creates a particle P and destroys its antiparticle $\bar{P}$ then the complex conjugate field $\psi^*$ should create the antiparticle $\bar{P}$ and destroy particle P [4, 5]. Therefore, a complex field solution of Dirac equation means that $\psi \neq \psi^*$ and implies the existence of antiparticles which are different from the particles. This fact leads to the discovery of the positron, the antiparticle of the electron.

Majorana then asks whether a spin $\frac{1}{2}$ particle might be its own antiparticle [5]. That is, he wants to find out the real field solutions to Dirac equation. He discovers the description of such fermion fields in 1937 [1]. His idea is to look for a representation in which all the $\gamma$ matrices are pure imaginary. One of such a representation is given by [6]:

$$\tilde{\gamma}^0 = \begin{pmatrix} 0 & \sigma^2 \\ \sigma^2 & 0 \end{pmatrix} \quad , \quad \tilde{\gamma}^1 = \begin{pmatrix} i\sigma^1 & 0 \\ 0 & i\sigma^1 \end{pmatrix}$$
$$\tilde{\gamma}^2 = \begin{pmatrix} 0 & \sigma^2 \\ -\sigma^2 & 0 \end{pmatrix} \quad , \quad \tilde{\gamma}^3 = \begin{pmatrix} i\sigma^3 & 0 \\ 0 & i\sigma^3 \end{pmatrix} \tag{1.4}$$

In this representation, the $(i\tilde{\gamma}^\mu \partial_\mu - m)$ is real in the Dirac equation Eq. (1.1) so it is natural to have solutions that satisfy the reality condition:

$$\psi = \psi^* \tag{1.5}$$

It is interesting to see what the reality condition means in the chiral representation. The two sets of $\gamma$ matrices are related to each other by a unitary transformation. After this transformation, we find out that the reality condition restricts the solutions of Dirac equation to take the following form [6]:

$$\psi(x) = \begin{pmatrix} \chi(x) \\ -i\sigma^2\chi^*(x) \end{pmatrix} \tag{1.6}$$

We can check that the above form of solutions indeed transform correctly under Lorentz transformations. If we write the Dirac spinor as $\psi = (\xi_L, \xi_R)^T$, Lorentz trans-

formation $\psi \to \Lambda_{\frac{1}{2}}\psi$ means the upper two components $\xi_L$ and lower two components $\xi_R$ transform like:

$$\xi_L \to \exp\left(-\frac{1}{2}\beta_k\sigma^k - \frac{i}{2}\theta_j\sigma^j\right)\xi_L$$
$$\xi_R \to \exp\left(\frac{1}{2}\beta_k\sigma^k - \frac{i}{2}\theta_j\sigma^j\right)\xi_R \tag{1.7}$$

One can show that $\sigma^2\xi_L^*$ transforms like $\xi_R$ therefore Eq. (1.6) is a legitimate solution of Dirac equation. In summary, the Majorana fields represent a certain set of solutions of Dirac equation under the reality condition. The particles associated with these real fields are their own antiparticles.

Although Majorana hopes that his Majorana fields might apply to some kinds of elementary particles like neutrinos, there is no experimental evidence to clearly prove that yet. However, after several decades, people find that the Majorana zero modes, which are analogs of Majorana fermions, can certainly exist as elementary excitations in solid state systems. The key idea is to introduce the superconductivity to these materials. Theoretically, the Bogoliubov-de Gennes (BdG) equation that describes the superconductivity in the materials with strong spin orbit coupling is similar to the Dirac equation. The particle hole symmetry and the zero energy condition of BdG equation play a similar role as the reality condition Eq. (1.5) of Dirac equation, thus under certain conditions the field operators corresponding to the zero energy solutions are their own Hermitian conjugates. That is,

$$\gamma^\dagger = \gamma \tag{1.8}$$

And these operators obey anticommutation relations:

$$\{\gamma_i, \gamma_j^\dagger\} = 2\delta_{ij} \tag{1.9}$$

It is natural to call the particles created or annihilated by these field operators Majorana fermions. In condensed matter context, we usually call them Majorana zero modes to emphasize that they correspond to low energy excitations in solid state systems. These Majorana zero modes are interesting not only because of their peculiar physical properties, but also because of their applications to topological quantum

computation. In the following sections, we will see how Majorana zero modes emerge from solid state systems and why it can be applied to topological quantum computation.

## 1.2 A toy model of Majorana fermions: Kitaev chain

A Majorana fermion may not be very interesting at first sight, since we can always define Majorana operators using the normal fermion operators $a^\dagger$, $a$:

$$\gamma_1 = a^\dagger + a \tag{1.10}$$

$$\gamma_2 = i(a^\dagger - a) \tag{1.11}$$

which means an ordinary electron can be roughly regarded as two paired Majorana fermions. However, if a system can support unpaired Majorana fermions, it may have interesting properties. Early in 2000, Read and Green proposed that unpaired Majorana fermions can emerge if the Cooper pairs have orbital angular momentum (p-wave superconductivity) [7]. The systems they suggested to host Majorana fermions are the 5/2 fractional quantum Hall states. These systems, however, are abstruse since they are not exactly solvable and rely on the suggesting Pfaffian or Moore-Read wavefuction [8]. In 2001, Kitaev put forward his famous toy model to explain the appearance of unpaired Majorana fermions [2]. This model is important, because it is a simple and exactly solvable one dimensional lattice model, nevertheless it can answer all of the following questions:

- What are the necessary ingredients to have unpaired Majorana fermions?
- What are the conditions to have unpaired Majorana fermions?
- Why are unpaired Majorana fermions topologically protected?
- Why are unpaired Majorana fermions useful for fault tolerant topological quantum computation?

- How to detect Majorana fermions?

In this section, I will mainly follow Kitaev's ideas in Ref. [2] to explain how these questions are answered.

Now let's consider Kitaev's lattice or tight binding model. Consider a chain with L cites, the Hamiltonian is

$$H = \sum_j [-t(a_j^\dagger a_{j+1} + a_{j+1}^\dagger a_j) - \mu a_j^\dagger a_j + \Delta a_j a_{j+1} + \Delta^* a_{j+1}^\dagger a_j^\dagger] \tag{1.12}$$

The first term describes the tunneling between two neighbor sites. The second term is the chemical potential. The last two terms describes the superconductivity. The superconductivity here is roughly p-wave since if we transform to the momentum space, it will have $ik$ terms in low momentum limit. We rewrite the Hamiltonian with the Majorana operators

$$c_{2j-1} = exp(i\theta/2)a_j + exp(-i\theta/2)a_j^\dagger \tag{1.13}$$

$$c_{2j} = -iexp(i\theta/2)a_j + iexp(-i\theta/2)a_j^\dagger \tag{1.14}$$

We can check that $c_{2j-1}$ and $c_{2j}$ satisfy the relations in Eq. (1.8) and Eq. (1.9). Now the Hamiltonian becomes:

$$H = \frac{i}{2}\sum_j [-\mu c_{2j-1}c_{2j} + (t + |\Delta|)c_{2j}c_{2j+1} + (-t + |\Delta|)c_{2j-1}c_{2j+2}] \tag{1.15}$$

To understand the physics behind this Hamiltonian in an easy way, we consider two limits in parameter space.

(1)The trivial phase: $|\Delta| = t = 0$ and $\mu < 0$. We have

$$H = -\mu\sum_j (a_j^\dagger a_j - \frac{1}{2}) = -\mu\frac{i}{2}\sum_j c_{2j-1}c_{2j} \tag{1.16}$$

This is the A phase shown in Fig. 1.1. Two Majorana operators from the same cite are paired together. This is trivial.

(2)The topological phase: $|\Delta| = t > 0$ and $\mu = 0$. We have

$$H = it\sum_j c_{2j}c_{2j+1} \tag{1.17}$$

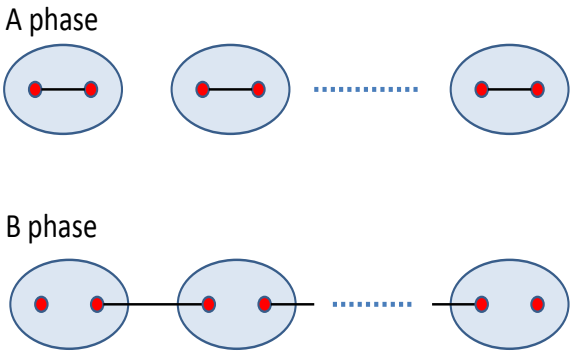


Figure 1.1. Two phases of the wire.

This is the B phase shown in Fig. 1.1. Majorana operators from different cite are paired together and leave two unpaired Majorana fermions at the ends of the chain. If we now define new fermionic operators: $b_j = \frac{1}{2}(c_{2j} + ic_{2j+1})$, $b_j^\dagger = \frac{1}{2}(c_{2j} - ic_{2j+1})$, the Hamiltonian

$$H = 2t \sum_{j=1}^{L-1} (b_j^\dagger b_j - \frac{1}{2}) \tag{1.18}$$

Therefore, the ground state has two fold degeneracy: $|\Psi_0\rangle$ and $|\Psi_1\rangle$. Using the unpaired majorana operators $c_1$, $c_{2L}$, we can characterize these two degenerate ground states by their fermionic parity, $P = -ic_1c_{2L}$:

$$-ic_1c_{2L}|\Psi_0\rangle = |\Psi_0\rangle, -ic_1c_{2L}|\Psi_1\rangle = -|\Psi_1\rangle \tag{1.19}$$

The ground states $|\Psi_0\rangle$ and $|\Psi_1\rangle$ are separated from the excited states by a gap $2t$. We can show that they are topologically protected, i.e., all local perturbations can not transform the state from $|\Psi_0\rangle$ to $|\Psi_1\rangle$ or vice versa. For example, if we have a perturbation: $V = \sum A_{ij}a_i^\dagger a_j$ but it doesn't contain both $a_1$ and $a_L$. When we express it with Majorana operators in Eq.(1.13) and (1.14) , we see that it at best contains one of $c_1$ and $c_{2L}$ thus the matrix element $\langle\Psi_0|V|\Psi_1\rangle = 0$. If a quantum bit is defined by these two ground states, then it is topologically protected since any local perturbation can not flip it.

Now let's consider the condition to realize Majorana fermions for arbitrary parameters. In order to find out the condition separating topologically different regimes, we consider the Hamiltonian in the momentum space

$$H = \sum_p \frac{1}{2}\Psi_p^\dagger \begin{pmatrix} -2tcosp-\mu & 2i\Delta^* sinp \\ -2i\Delta sinp & 2tcosp+\mu \end{pmatrix} \Psi_p \tag{1.20}$$

where $\Psi_p = (a_p, a_{-p}^\dagger)^T$. The energy spectrum is $E_\pm(p) = \pm\sqrt{(2tcosp+\mu)^2 + 4|\Delta|^2 sin^2 p}$. We will see that the energy gap closes when $|\mu| = |2t|$. We expect that the phase A and B in Fig.1.1 will extend to connected regions in the parameter space where the spectrum has a gap, therefore the trivial phase A occurs at $2|t| < |\mu|$ while the phase B with Majorana fermions occurs at $2|t| > |\mu|$. We can verify this conjecture by directly diagonalizing Hamiltonian Eq. (1.15). If it allows zero modes, these zero modes should have the forms:

$$\begin{aligned} \gamma_1 &= \sum_j (\alpha_1 s_+^j + \beta_1 s_-^j) c_{2j-1} \\ \gamma_2 &= \sum_j (\alpha_2 s_+^{-j} + \beta_2 s_-^{-j}) c_{2j} \\ s_\pm &= \frac{-\mu \pm \sqrt{\mu^2 - 4t^2 + 4|\Delta|^2}}{2(t+|\Delta|)} \end{aligned} \tag{1.21}$$

If we assume that the $\gamma_1$ mode localizes at the left and $\gamma_2$ mode localizes at the right, we also have the boundary condition:

$$\begin{aligned} \alpha_1 + \beta_1 &= 0 \\ \alpha_2 s_+^{-(L+1)} + \beta_2 s_-^{-(L+1)} &= 0 \end{aligned} \tag{1.22}$$

(1)For $2|t| < |\mu|$, we have $|s_+| > 1$, $|s_-| < 1$ or $|s_+| < 1$, $|s_-| > 1$, so only one of the $\alpha_1$, $\beta_1$ (or $\alpha_2$, $\beta_2$) can be non zero. The boundary conditions can not be satisfied, therefore there is no zero mode solution in this case.

(2)For $2|t| > |\mu|$ and $\Delta \neq 0$, we have $|s_+| < 1$, $|s_-| < 1$. The boundary conditions can be satisfied so we have unpaired Majorana fermions localized near the ends of the chain in this case.

The above analysis basically provides a paradigm to study the topological quantum phase transitions. We first find out the bulk spectrum of a system in parameter space. Then we divide the parameter space into several gapped regions by the lines where the gap closes. We can analyze the ground states degeneracy in different gapped regions to see if they allow the emergence of Majorana fermions or parafermions. A topological quantum phase transition may happen if the system evolves from a trivial region to the region with a non-trivial ground state degeneracy. We apply this method to study the hybrid superconductor/semiconductor systems in our work, which will be introduced in later chapters.

Systems with unpaired Majorana fermions can be used as qubits for fault tolerant quantum computation since they are intrinsically immune to decoherence [2, 9]. Quantum states are fragile because they are sensitive to errors of two kinds. A classical error flips the jth qubit changing $|0\rangle$ to $|1\rangle$ or vice versa. A phase error changes the sign of the states. The following scheme can be used to avoid the classical error. Let each qubit be a site that can be either empty or occupied by an electron, denoted by $|0\rangle$ and $|1\rangle$ respectively. Single classical errors become impossible because the electric charge is conserved(even in superconductor, the fermionic parity is conserved). Now the phase error which is represented by $a^\dagger a$ may occur. But if we introduce the Majorana operators given by Eq.(1.10),(1.11), the phase error:

$$a^\dagger a = \frac{1}{2}(1 + i\gamma_1\gamma_2) \tag{1.23}$$

It involves the interaction from two Majorana fermions. So if we can have isolated Majorana fermions, both two kinds of errors can be avoided. Furthermore, Majorana fermions have non-Abelian statistics. Braiding Majorana fermions can lead to nontrivial quantum evolutions of the ground states. A ground state subspace that is immune to decoherence and the capability to do quantum operations within the ground state subspace, make Majorana fermions useful for topological quantum computation.

To close this section, let's discuss how to detect the Majorana fermions. Here I will introduce the scheme that is first shown by Kitaev [2], the fractional Josephson

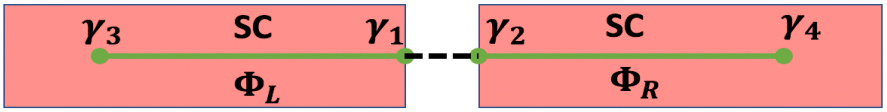


Figure 1.2. A superconductor-insulator-superconductor junction. Red regions indicate s-wave superconductors (with phases $\phi_L, \phi_R$) that drives the green regions into a 1D topological state. The dashed region is trivially gapped. The Majorana fermions mediate a component of the Josephson current that is $4\pi$ periodic in $\phi_R - \phi_L$ [10].

effect. I will show that the Josephson current has a $4\pi$ periodicity component between two topological superconductors which host Majorana fermions. The argument I used here is the same as Ref. [10]. The schematic experimental setup is plotted in Fig. 1.2. Two topological 1D superconductor regions are separated by an insulating barrier represented by a dashed line. We assume that these 1D wires are long enough such that the overlap between the outer Majorana fermions $\gamma_{3,4}$ and the inner $\gamma_{1,2}$ is very small. But the insulating barrier must be very narrow so $\gamma_1$ and $\gamma_2$ hybridize strongly. We now derive the zero-bias Josephson current when we vary the phase difference $\Delta\phi = \phi_R - \phi_L$.

The total current contains two parts. $I = I_{2e} + I_e$. The $I_{2e}$ denotes the normal Josephson effect and is $2\pi$ periodic in $\Delta\phi$. We just need to discuss $I_e$. To simplify the derivation, we assume that the two wires are two N-cite chains describing by Kitaev's toy model, which is discussed in the last section. We also tune $\mu = 0$ and $t = \Delta$ so that $\gamma_1$ and $\gamma_2$ are isolated from the bulk Hamiltonian. We define $c^\dagger_{L/Rx}$ operator that adds electrons to the left/right segment at cite x. The Hamiltonian can be written as

$$H = \sum_{a=L/R} H_a + H_\Gamma \tag{1.24}$$

We have

$$H_a = -t \sum_{x=1}^{N-1} (c^\dagger_{ax} c_{ax+1} + e^{i\phi_a} c_{ax} c_{ax+1} + H.c.) \tag{1.25}$$

$$H_\Gamma = -\Gamma (c^\dagger_{LN} c_{R1} + H.c.) \tag{1.26}$$

The $H_\Gamma$ describes single electron tunneling through the barrier with strength $\Gamma > 0$. According to the discussion in the Kitaev's toy model, the lattice fermion operators can be written with Majorana operators:

$$c_{LN} = e^{-i\phi_L/2}(\gamma_1 + i\gamma_1')/2, c_{R1} = e^{-i\phi_R/2}(\gamma_2' + i\gamma_2)/2 \tag{1.27}$$

where $\gamma_1', \gamma_2'$ are neighboring cites. We can project the $H$ onto the ground state subspace of $H_a$. Note that the $\gamma_1', \gamma_2'$ can be written in the form of $b^\dagger + b$ and their matrix elements in the ground state subspace are zero. Therefore, the projection means: $H_a \to 0, c_{LN} \to \frac{1}{2}e^{-i\phi_L/2}\gamma_1, c_{R1} \to \frac{i}{2}e^{-i\phi_R/2}\gamma_2$. The effective Hamiltonian is

$$H_{eff} = \frac{\Gamma}{2}cos(\frac{\Delta\phi}{2})i\gamma_1\gamma_2 = -\Gamma cos(\frac{\Delta\phi}{2})(n_1 - 1/2) \tag{1.28}$$

where $n_1 = b^\dagger b$ and $b^\dagger = \frac{1}{2}(\gamma_1 - i\gamma_2)$. For superconductors, we have a commutation relation for phase $\phi$ and the particle number $N$:

$$[\frac{\hbar}{2}\phi, N] = [\frac{\hbar}{2}\phi, \frac{2}{i}\frac{\partial}{\partial\phi}] = i\hbar \tag{1.29}$$

Therefore, they are Hermitian conjugate operators. Applying the Hamilton equation, we have the current $I_e$ (right as positive):

$$I_e = -e\frac{dN_R}{dt} = e\frac{\partial H_{eff}}{\partial(\frac{\hbar}{2}\phi_R)} = \frac{2e}{\hbar}\frac{H_{eff}}{d\Delta\phi} = \frac{e\Gamma}{2\hbar}sin(\frac{\Delta\phi}{2})(2n_1 - 1) \tag{1.30}$$

From the above equation, we see that $I_e$ is $4\pi$ periodic in $\Delta\phi$. Measuring the $4\pi$ periodic contribution is a convincing evidence for the existence of Majorana fermions. Furthermore, as the sign of Eq. (1.30) is related to $n_1$ which represents the qubit state of $\gamma_1$ and $\gamma_2$, this method also enables qubit readout. Experimentally, this fractional Josephson effect is confirmed by the Shapiro step measurements [11].

### 1.3 Non-Abelian statistics of Majorana fermions

The non-Abelian statistics is a special property of Majorana fermions and parafermions that makes them useful for topological quantum computation. Before discussing the non-Abelian statistics, I want to explain why richer exchange statistics are allowed for

low dimensional systems. The possibility to have anyons in low dimensional systems is first pointed out by Ref. [12]. They argue that the exchange statistics is related to the concept of identical particles and the topology of the configuration space. Here I will follow a simplified version of argument given by Wen to explore the exchange statistics in 2D and 3D spaces [13].

First let me introduce the local phase and the global phase. The local phase is related to the contractible loops (loops that can be continuously shrunk to a point). It is given by:

$$\Phi_{local} = \exp\left(ie \oint \mathbf{A} d\mathbf{x}\right) = \exp\left(ie \int \mathbf{B} \cdot d\mathbf{S}\right) \tag{1.31}$$

The $\mathbf{B}$ can be magnetic field or Berry curvature. The global phase is associated with non-contractible loops. When a non contractible loop is shrunk, it will encounter one or more singular points. Let's assume there is only one singular point and we can attach a flux tube to it which generates phase $e^{ie\phi}$. So, the global phase can be:

$$\Phi_{global} = e^{ien_w\phi} \tag{1.32}$$

where $n_w$ is the winding number of the loop around the singularity.

Now consider two identical particles in a three or two dimensional space where the local phase is zero. Because $(\mathbf{r}_1, \mathbf{r}_2)$ and $(\mathbf{r}_2, \mathbf{r}_1)$ should be regarded as the same point, the configuration space is then written as $V_+ \otimes V_-$. The $V_+$ is the whole three or two dimensional space, while $V_-$ is $\{\mathbf{r}_-|\mathbf{r}_- \neq 0, \mathbf{r}_- \sim -\mathbf{r}_-\}$ with $\mathbf{r}_- = \mathbf{r}_1 - \mathbf{r}_2$. $V_-$ can be thought of as half of the whole space with the origin removed, $\mathbf{r}$ and $-\mathbf{r}$ sticked together.

For two particles in three dimensional space, $V_-$ is not simply connected, so a global phase can exists. The red loop on the left of Fig. 1.3 represent an exchange of two particles since it connects $\mathbf{r}$ to $-\mathbf{r}$. It is non-contractible so we can attach to it a global phase $e^{i\theta}$. The red loop on the right of Fig. 1.3 can be attached a global phase $e^{-i\theta}$ since it goes in opposite direction. However, the left and right loops can be continuously transformed to each other by rotating around the z axis. We have

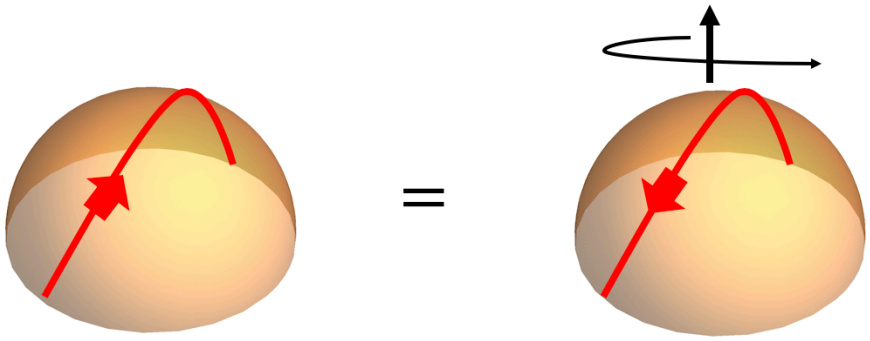

Figure 1.3. The red exchange loop on the left is a non-contractible loop, but it can be continuously transformed to the red exchange loop on the right by rotating about the z axis.

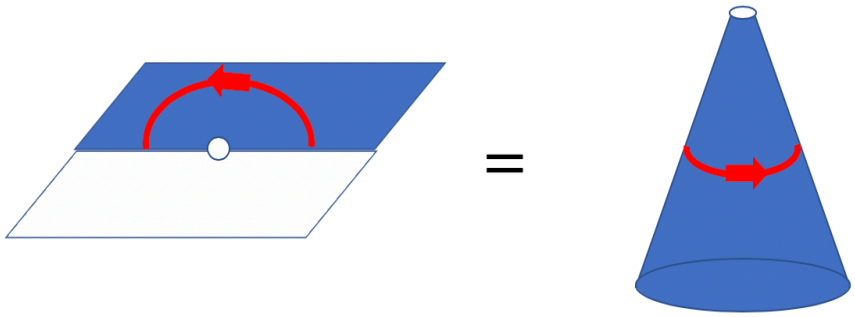

Figure 1.4. The blue regions on left and right represent $V_{-}$. The red curve represent a non-contractible exchange path with winding number $n_w = 1$. [13]

$e^{i\theta} = e^{-i\theta}$. There are only two possibilities: $\theta = 0$ which represents bosons and $\theta = \pi$ which represents fermions. Therefore, we do not have anyons in three dimensional space.

Now let's look at the two dimensional space. The space $V_{-}$ is represented by the blue regions in Fig. 1.4. The global phase attached to the exchange of two identical particles is $e^{i\theta}$. Now there is no restriction to $\theta$. We can have anyons if $\theta$ takes values other than 0 and $\pi$.

Majorana fermions can have more exotic exchange statistics, the non-Abelian statistics, in space dimension lower than three. From the last section, we see that two unpaired Majorana fermions means two fold degeneracy of the ground state. If we have a collection of 2N Majorana fermions, we will have $2^N$ fold degenerate ground states. The non-Abelian statistics of this system means the following thing: We start from a state in the ground state subspace, then perform sequential exchanges of Majorana fermions, the final state depends on the order of the exchanges. It is first proposed by Moore and Read [8] in fractional quantum hall effect. Then Ivanov discussed it in the 2D spinless $p + ip$ superconductor [14]. Here I will follow the arguments in [10, 15]. I first present the approximate solution of the bound state in a vortex of p-wave superconductor and show how exchanging two vortices leads to

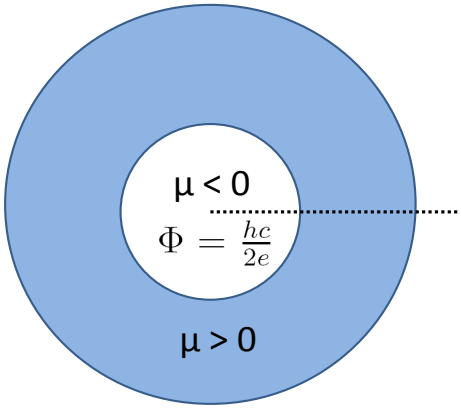


Figure 1.5. Vortex in p-wave superconductor

unusual changes to Majorana operators. Then I will discuss the emergent non-Abelian statistics.

Now let's consider a 2D spinless $p + ip$ superconductor. A quantum flux $\Phi = \frac{hc}{2e}$ threads the central trivial region with chemical potential $\mu < 0$ and radius $R_i$. The outer region has chemical potential $\mu > 0$ and radius $R_o$. We know from previous sections that an edge mode will appear on the boundary. It is illustrated in Fig. 1.5. The Hamiltonian describing this system is

$$H = \int d^2r\{\psi^\dagger(-\frac{\nabla^2}{2m} - \mu)\psi + \frac{\Delta}{2}[e^{-i\theta}e^{i\phi}\psi(\partial_x + i\partial_y)\psi + H.c.]\} \tag{1.33}$$

We attach two phase factors to the pairing amplitude. The first one $e^{-i\theta}$ comes from the flux quantum which generates this vortex. The $\theta$ here is the azimuth angle in polar coordinate. The second one $e^{i\phi}$ comes from the other sources such as the other vortices and here for solving single vortex problem we just assume that it is a constant. We also assume that $\Delta$ is a constant since we are only interested in the edge modes.

The $-\frac{\nabla^2}{2m}$ is also discard for the same reason. Now, the Hamiltonian in the polar coordinate is:

$$\begin{aligned} H &= \frac{1}{2}\int d^2r\Psi^\dagger(r)H_{BdG}\Psi(r) \\ &= \frac{1}{2}\int d^2r\Psi^\dagger(r)\begin{pmatrix} -\mu(r) & \Delta e^{-i\phi}(-\partial_r + \frac{i\partial_\theta}{r}) \\ \Delta e^{i\phi}(\partial_r + \frac{i\partial_\theta}{r}) & \mu(r) \end{pmatrix}\Psi(r) \end{aligned} \tag{1.34}$$

where $\Psi^\dagger(r) = [\psi^\dagger(r), \psi(r)]$. Now we need to find the edge state wavefunction which satisfies $H_{BdG}\chi(r) = E\chi(r)$. We assume the following form of the wavefunction

$$\chi_n(r) = e^{in\theta}\begin{pmatrix} e^{-i\phi/2}[f(r) + ig(r)] \\ e^{i\phi/2}[f(r) - ig(r)] \end{pmatrix} \tag{1.35}$$

We find that the functions $f$ and $g$ obey

$$\begin{aligned} (E + n\Delta/r)f &= -i[\mu(r) - \Delta\partial_r]g, \\ (E - n\Delta/r)g &= i[\mu(r) + \Delta\partial_r]f \end{aligned} \tag{1.36}$$

Since we are considering the edge states, we assume that $r \to R_i$ is a constant for the inner edge. We have the inner edge states energies and wavefunctions which are given by

$$E_n = -\frac{n\Delta}{R_i} \tag{1.37}$$

$$\chi_n(r,\theta) = e^{in\theta}e^{-\frac{1}{\Delta}\int_{R_i}^{r} dr'\mu(r')}\begin{pmatrix} e^{-i\phi/2} \\ e^{i\phi/2} \end{pmatrix} \tag{1.38}$$

Therefore, for the zero energy mode, the Majorana operator is:

$$\Gamma_0 = A\int d^2r e^{-\frac{1}{\Delta}\int_{R_i}^{r} dr'\mu(r')}(e^{-i\phi/2}\psi^\dagger(r) + e^{i\phi/2}\psi(r)) \tag{1.39}$$

where A is a normalization constant. We can see from the above expression that if the superconducting phase changes from $\phi$ to $\phi + 2\pi$, the pairing amplitude does not change, but Majorana operator will change sign. We need to restrict the phase in the

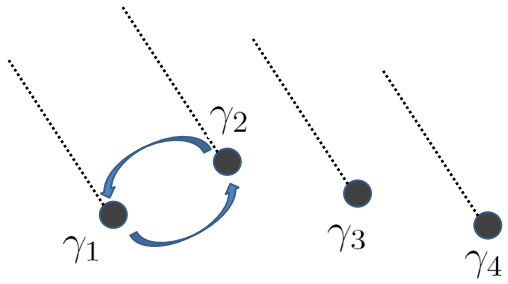


Figure 1.6. Four well separated vortices binding Majorana zero modes

interval $[0, 2\pi)$ and introduce branch cuts to indicate where the phase jumps by $2\pi$. In Fig. 1.5, the dash line represents the branch cut from the $hc/2e$ flux.

Let's consider four vortices as shown in Fig. 1.6. Now if we consider the exchange of two vortices represented by $\gamma_1$ and $\gamma_2$ in the way as Fig. 1.6, from the previous discussion, we know the change of the operators is: $\gamma_1 \to \gamma_2$ and $\gamma_2 \to -\gamma_1$. For a general exchange $T_{ij}$ of $\gamma_i$ and $\gamma_j$, we hope to achieve the operator change: $\gamma_i \to \gamma_j$, $\gamma_j \to -\gamma_i$ and $\gamma_k \to \gamma_k$ for all $k \neq i, j$. We find that the following operator can do this

$$\tau(T_{ij}) = exp(\frac{\pi}{4}\gamma_j\gamma_i) = \frac{1}{\sqrt{2}}(1 + \gamma_j\gamma_i) \tag{1.40}$$

We can see that it is what we need by directly calculating the $\tau(T_{ij})\gamma_k\tau^{-1}(T_{ij})$. For four vortices with Majorana operators $\gamma_1, \gamma_2, \gamma_3, \gamma_4$, we pair them into complex fermion operators:

$$\begin{aligned} a &= \frac{1}{2}(\gamma_1 + i\gamma_2), a^\dagger = \frac{1}{2}(\gamma_1 - i\gamma_2) \\ b &= \frac{1}{2}(\gamma_3 + i\gamma_4), b^\dagger = \frac{1}{2}(\gamma_3 - i\gamma_4) \end{aligned} \tag{1.41}$$

The basis vectors of the ground state subspace can be written as $|00\rangle, |11\rangle, |10\rangle, |01\rangle$. The first number is the occupation number for operator $a$ and the second for $b$. Then,

the representation of exchange of 12,23,34 Majorana operators can be written in terms of the complex fermion operators:

$$\begin{aligned}
\tau(T_{12}) &= \frac{1}{\sqrt{2}}(1 - i(aa^\dagger - a^\dagger a)) \\
\tau(T_{14}) &= \frac{1}{\sqrt{2}}(1 - i(ba + ba^\dagger - b^\dagger a - b^\dagger a^\dagger)) \\
\tau(T_{34}) &= \frac{1}{\sqrt{2}}(1 - i(bb^\dagger - b^\dagger b))
\end{aligned} \tag{1.42}$$

The explicit matrix representation of them is

$$\tau(T_{12}) = \frac{1}{\sqrt{2}} \begin{pmatrix} 1-i & 0 & 0 & 0 \\ 0 & 1+i & 0 & 0 \\ 0 & 0 & 1+i & 0 \\ 0 & 0 & 0 & 1-i \end{pmatrix} \tag{1.43}$$

$$\tau(T_{14}) = \frac{1}{\sqrt{2}} \begin{pmatrix} 1 & -i & 0 & 0 \\ -i & 1 & 0 & 0 \\ 0 & 0 & 1 & i \\ 0 & 0 & i & 1 \end{pmatrix} \tag{1.44}$$

$$\tau(T_{34}) = \frac{1}{\sqrt{2}} \begin{pmatrix} 1-i & 0 & 0 & 0 \\ 0 & 1+i & 0 & 0 \\ 0 & 0 & 1-i & 0 \\ 0 & 0 & 0 & 1+i \end{pmatrix} \tag{1.45}$$

We see that in this basis, the $T_{14}$ has off-diagonal matrix elements so it does not commute with the other two. This is the reason we call it non-Abelian statistics. Braiding the Majorana fermions can achieve non-trivial quantum operations, which can be used for topological quantum computation.

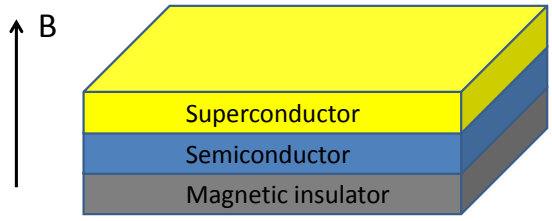


Figure 1.7. Schematic picture of the heterostructure hosting Majorana zero mode inside the ordinary vortex.

## 1.4 Majorana fermions in semiconductor systems

In this section, I will review a conventional semiconductor system which hosts Majorana fermions proposed by S. Das Sarma's group [16]. They show that a film of a semiconductor in which s-wave superconductivity and Zeeman splitting are induced by proximity effect, supports the Majorana zero mode in the ordinary vortex. This is also an example of achieving p-wave spinless superconductor in a real system. The s-wave superconductivity can be transformed in to p-wave with spin orbit interaction in the semiconductor thin film. The Zeeman splitting open a gap in the bulk spectrum and thus by choosing suitable chemical potential, only a single effective "spinless" band needs to be considered. I will include their detailed proof of the existence of Majorana fermions since We are going to use similar methods for our research in the hole doped systems.

The system to be considered is shown in Fig. 1.7. The thin film is sandwiched between the superconductor and Magnetic insulator.The single particle Hamiltonian for conduction band of the semiconductor thin film is

$$H_0 = \frac{p^2}{2m} - \mu + V_z\sigma_z + \alpha(\vec{\sigma} \times \vec{p}) \cdot \hat{z} \tag{1.46}$$

where $V_z$ is the effective Zeeman coupling induced by the magnetic insulator. The superconducting Hamiltonian is given by $H_{SC} = \int d^2r(\Delta_0\psi_\uparrow\psi_\downarrow + H.c.)$. The BdG equation is [16]:

$$\begin{pmatrix} H_0 & \Delta_0(\mathbf{r}) \\ \Delta_0^*(\mathbf{r}) & -\sigma_y H_0^* \sigma_y \end{pmatrix} \Psi(\mathbf{r}) = E\Psi(\mathbf{r}) \tag{1.47}$$

As we are considering the vortex in the heterostructure, the order parameter $\Delta_0(\mathbf{r}) = \Delta_0(r)e^{i\theta}$. The wavefunction should take the following form

$$\Psi_m(r,\theta) = e^{im\theta}[u_\uparrow(r), u_\downarrow(r)e^{i\theta}, v_\downarrow(r)e^{-i\theta}, -v_\uparrow(r)]^T \tag{1.48}$$

The BdG equation is particle-hole symmetric. It means that if $\Psi_m(\mathbf{r})$ is a solution with energy $E$, the $i\sigma_y\tau_y\Psi_m^*(\mathbf{r})$ is also a solution at energy $-E$ in the angular momentum channel $-m$. $\tau_y$ is the Pauli matrix in the particle hole space. Thus, a zero energy solution can be non-degenerate only if it exists in the $m = 0$ channel. In this case the corresponding quasiparticle operator is guaranteed to be a Majorana operator by the particle-hole symmetry. Again, because of the particle-hole symmetry, we only need to consider a reduced spinor $\Psi_0(r) = [u_\uparrow(r), u_\downarrow(r)]^T$ and $[v_\uparrow(r), v_\downarrow(r)]^T = \lambda[u_\uparrow(r), u_\downarrow(r)]^T$. The reduced BdG equation is [16]:

$$\begin{pmatrix} -\eta(\partial_r^2 + \frac{1}{r}\partial_r) + V_z - \mu & \lambda\Delta_0(r) + \alpha(\partial_r + \frac{1}{r}) \\ \lambda\Delta_0(r) - \alpha\partial_r & -\eta(\partial_r^2 + \frac{1}{r}\partial_r - \frac{1}{r^2}) - V_z - \mu \end{pmatrix} \Psi_0(r) = 0 \tag{1.49}$$

We can assume that $\Delta_0(r) = 0$ for $r < R$ and $\Delta_0(r) = \Delta_0$ for $r \geq R$. So for $r < R$, the analytical solution is $\Psi_0(r) = [u_\uparrow J_0(zr), u_\downarrow J_1(zr]^T$ where $J_n$ are Bessel functions of the first kind with the constraint

$$\begin{pmatrix} \eta z^2 + V_z - \mu & z\alpha \\ z\alpha & \eta z^2 - V_z - \mu \end{pmatrix} \begin{pmatrix} u_\uparrow \\ u_\downarrow \end{pmatrix} = 0 \tag{1.50}$$

Since the Bessel functions are symmetric, we use the roots of characteristic equation $\pm z_1, \pm z_2$ to find two solutions which are well behaved at the origin: $\Psi_1(r) = [u_\uparrow J_0(z_1 r), u_\downarrow J_1(z_1 r]^T$, $\Psi_2(r) = [u_\uparrow J_0(z_2 r), u_\downarrow J_1(z_2 r]^T$. The full solution for $r < R$ is

$\Psi_0(r) = c_1\Psi_1(r) + c_2\Psi_2(r)$.

For $r > R$, we can write the solution to Eq.(1.49) as

$$\Psi_0(r) = \frac{e^{izr}}{\sqrt{r}} \sum_{n=0,1,2...} \frac{a_n}{r^n} \tag{1.51}$$

We just need to consider $a_0$ since higher order coefficients can be calculated from $a_0$ using recursion relations. $a_0$ satisfies

$$\begin{pmatrix} \eta z^2 + V_z - \mu & \lambda\Delta_0 + iz\alpha \\ -\lambda\Delta_0 - iz\alpha & \eta z^2 - V_z - \mu \end{pmatrix} a_0 = 0 \tag{1.52}$$

The characteristic equation is

$$\eta^2 z^4 - (2\mu\eta + \alpha^2)z^2 + 2i\lambda\alpha\Delta_0 z + \mu^2 + \Delta_0^2 - V_z^2 = 0 \tag{1.53}$$

In order to obtain a unique solution for the zero energy state, the number of the unknown coefficients should equal the number of the constraints. For a two component spinor, the boundary conditions are 4 at $r = R$ and we still have one normalization condition. So the number of constraints is 5. We already have two unknown coefficients for $r < R$, so we need three independent solutions for $r > R$. Analyzing the characteristic equation Eq. (1.53) using Vieta's theorem and note that for a bound state $Im[z] > 0$, we can see that the condition is $\lambda = 1$ and $V_z^2 > \mu^2 + \Delta_0^2$. We conclude that a Majorana zero mode exists in the vortex when the so called topological criterion is satisfied [16]:

$$V_z^2 > \mu^2 + \Delta_0^2 \tag{1.54}$$

Using similar methods, we can find that the same topological criterion holds for one dimensional system. Surprisingly, we will see that a similar topological criterion holds even for hole doped systems.

# 2. MAJORANA FERMIONS IN CHARGE CARRIER HOLE SYSTEMS

In this chapter, I will present our work for the spin orbit couplings and the emergence of Majorana fermions in charge carrier hole systems. I first review the band structure and the general spin orbit couplings of hole systems. Then I consider the Luttinger holes in quantum wells. The ground sub-bands of this system reflect the mutual transformation of heavy and light holes at the heteroboundaries. The effective two and one dimensional Hamiltonian is derived for the relevant two ground sub-bands. Using the effective Hamiltonian for quantum wires, I study the conditions for the realization of Majorana zero modes. I also discuss the possible candidate materials which can host Majorana zero modes. This work is published in Ref. [17].

## 2.1 Introduction

Electron band-structure and spin-orbit effects may lead to remarkable quantum matter such as topological insulators and topological superconductivity [18–21]. Many researchers studied charge carrier hole systems anticipating strong spin-orbit effects. However, in low-dimensional systems, in which spin-orbit interactions are well known for electrons, their understanding for holes is scarce and is just emerging [22, 23].

In our work, we derive a two-dimensional (2D) hole Hamiltonian, including g-factor and spin-orbits constants crucial for spintronics and quantum computing. The difference between holes and electrons are not just parameters, holes are special physical species with different symmetry and different ways of tuning their properties. We consider holes in quantum wires, which are lithographically or electrostatically defined in quantum wells, or developed using cleaved edge overgrowth, which differ from hole epitaxial and core-shell nanowires [24–26].

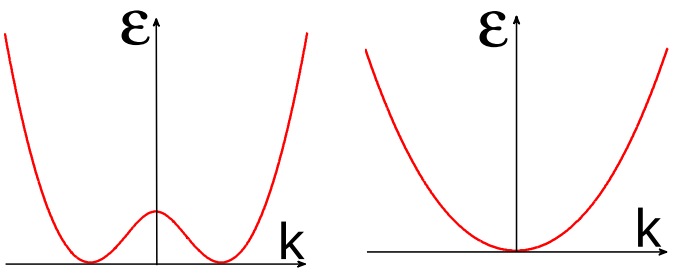


(a) (b)

Figure 2.1. a: Ground spin-orbit state energy at $E_{so} > g\mu H$. b: Ground spin orbit energy at $E_{so} < g\mu H$.

Using our results for 2D holes we discuss Majorana bound states (MBS) in wires. As reviewed in the last chapter, Majorana particles are their own anti-particles obeying non-Abelian statistics and promising for quantum computing [9, 27, 28]. Kitaev's model tells us that Majorana modes arise in p-wave spinless superconductors [2, 29]. Many schemes generating such superconductivity in semiconductor-superconductor structures use three ingredients: proximity effects, time reversal symmetry breaking, and spin-orbit coupling [10, 16, 20, 21, 30–32]. Spin orbit couplings not only tune the s-wave superconductivity into p-wave superconductivity, but stronger spin-orbit interaction also gives stronger p-wave pairing as the effective p-wave pairing amplitude is proportional to [32]:

$$f_p(k) = \frac{\gamma k}{2\sqrt{V_z^2 + \gamma^2 k^2}} \tag{2.1}$$

where $\gamma$,$V_z$ and $k$ denote the spin-orbit constant, Zeeman splitting and momentum respectively. Both electrons and hole systems were suggested for realizing Majorana modes [10, 25, 33, 34].

We show that in hole wires, the momentum-dependent Zeeman (spin-orbit) fields emerge in three spatial directions. This provides an opportunity to control the MBS by changing a relative orientation of spin-orbit and applied magnetic fields using electrostatic gates. Furthermore, at Zeeman energies $g\mu H$ satisfying conditions for

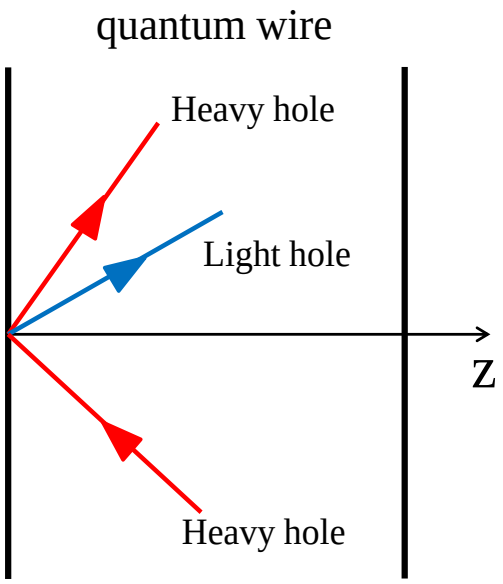


Figure 2.2. A schematic picture of transformation of holes reflected from the potential walls of the quantum wire

topological state, holes exhibit sizable spin-orbit energies $E_{so} = \gamma^2 m > g\mu H$, where $m$ is the effective mass. Then the hole ground state has a camel back shape, Fig.2.1(a), making p-pairing much stronger than in electron settings, see Eq.(2.1). For $E_{so} = \gamma^2 m < g\mu H$, the p-pairing is suppressed, Fig.2.1(b).

Our work is important not only for the realizations of Majorana zero modes, but also for the study of low dimensional holes. Most authors treat holes like electrons [34–39]: if the motion of particles is quantized in direction $i$ in a well of width $d$, their Hamiltonian is solved by replacing momentum $p_i$ by zeros and $p_i^2$ by its expectation value in the ground state, $\langle \hat{p_i^2} \rangle = (\frac{\hbar\pi}{d})^2$, and spin-orbit and Zeeman terms are found perturbatively. However, this approach is flawed. It does not account for a mutual transformation of heavy and light holes upon reflection from the heteroboundaries, Fig.2.2. Although this effect can be evaluated perturbatively by including off-diagonal terms linear in $k_i$, it then requires summation of an infinite number of terms, which are parametrically all the same [23]. An alternative non-perturbative approach is known since the work of Nedorezov [40], but is seldom used [23, 41–43]. We show

that in hole wires, this phenomenon strongly affects effective masses, g-factor and spin-orbit constants. Our treatment of 2D holes may lead to new interesting physics, and emergence of Majorana zero modes is just one example.

## 2.2 Hole Hamiltonian and spin orbit coupling

In this section, I will briefly introduce the band structure of the topmost valence band of GaAs, since our research study mainly the heavy and light hole states of this band. I will also review the spin orbit couplings.

For the band structure, we need to find our the dispersion relation $E_n(\mathbf{k})$ for the band we consider. One way to obtain this is the $k \cdot p$ method [44, 45]. In the crystal lattice, the potential is periodic so the wavefunctions take the Bloch form $\psi_{\mathbf{nk}}(\mathbf{r}) = e^{i\mathbf{kr}}u_{\mathbf{nk}}(\mathbf{r})$. The Hamiltonian consists of kinetic energy operator, a local periodic crystal potential and the spin orbit interaction term:

$$H = \frac{p^2}{2m} + V(\mathbf{r}) + \frac{\hbar}{4m^2c^2}(\sigma \times \nabla V) \cdot \mathbf{p} \tag{2.2}$$

The Schrodinger equation reads

$$H\psi_{\mathbf{nk}}(\mathbf{r}) = E_n(\mathbf{k})\psi_{\mathbf{nk}}(\mathbf{r}) \tag{2.3}$$

Moving the term $e^{i\mathbf{kr}}$ to the left of the above equation, we have an equation for the cellular functions $u_{\mathbf{nk}}(\mathbf{r})$:

$$H = \frac{p^2}{2m} + V(\mathbf{r}) + \frac{\hbar^2k^2}{2m} + \frac{\hbar}{m}\mathbf{k} \cdot (\mathbf{p} + \frac{\hbar}{4mc^2}\sigma \times \nabla V) + \frac{\hbar}{4m^2c^2}(\sigma \times \nabla V) \cdot \mathbf{p} \tag{2.4}$$

We can solve Eq.(2.4) in the band edge (normally $k = 0$) and obtain a complete orthonormal basis $u_{\mathbf{nk}}(\mathbf{r})$. Then we can regard the term $\frac{\hbar}{m}\mathbf{k} \cdot (\mathbf{p} + \frac{\hbar}{4mc^2}\sigma \times \nabla V)$ as perturbation to obtain the dispersion relation $E_n(\mathbf{k})$ for every $\mathbf{k}$. However, as there are infinite bands, it's hard to consider the effects of all of them. Usually we only need to consider several bands near the band which we are interested in. In our problem, we need to consider the topmost valence band. It is sufficient to consider the band

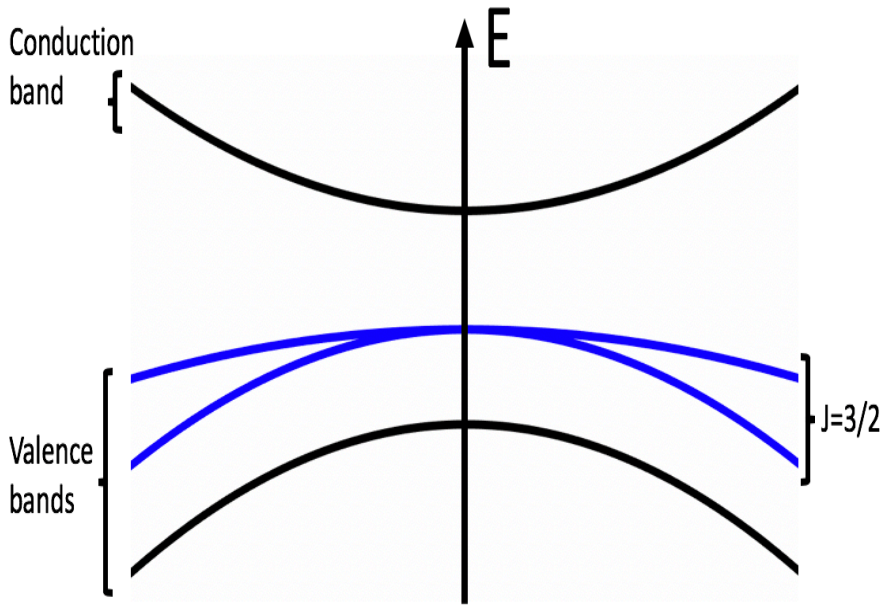


Figure 2.3. A schematic plot of the band structure of GaAs, or a general Zinc blende type material. The blue curves denote the topmost valence band which is described by the Luttinger Hamiltonian.

structure of GaAs which includes the effects of the p-like valence bands and the s-like conduction bands as shown in Fig.2.3. For the $\Gamma_8$ block consisting the topmost fourfold degenerate valence band, which is denoted blue in Fig.2.3, the dispersion up to the order of $k^2$ is described by the Luttinger Hamiltonian [46]:

$$H_L = \frac{1}{2m_0}[(\gamma_1 + \frac{5}{2}\gamma_2)p^2 - 2\gamma_3(\mathbf{J}\cdot\mathbf{p})^2 + 2(\gamma_3 - \gamma_2)(J_x^2 p_x^2 + c.p.)] \tag{2.5}$$

where $\gamma_1, \gamma_2, \gamma_3$ are Luttinger parameters and *c.p.* stands for cyclic permutations. $J_i$ is the j=3/2 representation of the generator of SU(2).

Now, let's move on to the spin orbit couplings. In semiconductors, the combined effect of inversion symmetry and time reversal symmetry lead to spin degeneracy. The proof is straightforward [45]. The time reversal symmetry implies that both the wave vector and the spin components of a state change sign:

$$E_+(\mathbf{k}) = E_-(-\mathbf{k}) \tag{2.6}$$

The inversion symmetry only changes the sign of the wave vector:

$$E_\pm(\mathbf{k}) = E_\pm(-\mathbf{k}) \tag{2.7}$$

Their combined effect is the spin degeneracy:

$$E_+(\mathbf{k}) = E_-(\mathbf{k}) \tag{2.8}$$

Therefore, if both symmetries are present, the spin states are degenerate. Here I will discuss the effect of the breaking of inversion symmetry. From Eq.(2.7), we observe that the odd power terms in $\mathbf{k}$ can not appear in the dispersion relations if inversion symmetry is preserved. In quasi-2D quantum wells and heterostructures, the spin splitting can be the consequence of a bulk inversion asymmetry (BIA) of the underlying crystal (e.g. a zincblende structure), or of a structure inversion asymmetry (SIA) of the confinement potential (e.g. electric field). Using the method of invariants, the Dresselhaus term which represents the cubic k contribution arising from the BIA can be written as [42]

$$H_D = \alpha_v(\mathbf{J}\cdot\kappa) + \frac{1}{2}\delta\alpha_v(\frac{13}{4}\mathbf{J}\cdot\kappa - \sum_j J_j^3\kappa_j + \sum_j V_j p_j(p_j^2 - \frac{1}{3}p^2)) \tag{2.9}$$

where $V_z = J_x J_z J_x - J_y J_z J_y$ and $\kappa_z = p_z(p_x^2 - p_y^2)$, other components can be obtained by cyclic permutations.

The Rashba term arising from the SIA [44]

$$H_R = \zeta(\mathbf{J} \times \mathbf{p}) \cdot \partial_{\mathbf{r}} U_e(z, \mathbf{r}) + \varrho(\mathcal{J} \times \mathbf{p}) \cdot \partial_{\mathbf{r}} U_e(z, \mathbf{r}) \tag{2.10}$$

where $\mathcal{J} = (J_x^3, J_y^3, J_z^3)$. In the above equation, we ignore the other terms which are several orders of magnitude smaller than the above two terms. In the next section, I will show that the heavy and light hole transformation, Dresselhaus and Rashba spin splitting have important effect on the hole spectrum of the quantum wire.

## 2.3 Effective Hamiltonians

In this section, I will derive the effective two and one dimensional Hamiltonians for the hole systems. We start from the Luttinger Hamiltonian Eq. (2.5) for the bulk holes. In an infinite symmetric well, the wavefunctions of Eq. (2.5), $\varphi_+(z, \mathbf{r})$ and $\varphi_-(z, \mathbf{r})$, $\mathbf{r} = (x, y)$, are symmetric and antisymmetric with respect to $z \to -z$ reflection. In the basis of Bloch functions $u^{3/2}, u^{1/2}, u^{-1/2}, u^{-3/2}$ of bulk holes, $\varphi^{\mathbf{k}}_{+,-}(z, \mathbf{r}) = \varphi^{\mathbf{k}}_{+,-}(z) exp(i\mathbf{k} \cdot \mathbf{r})$, and [43]:

$$\varphi^{\mathbf{k}}_{+}(z) = \begin{pmatrix} A_0 C_z \\ -iA_1 S_z e^{i\phi_k} \\ A_2 C_z e^{2i\phi_k} \\ -iA_3 S_z e^{3i\phi_k} \end{pmatrix}, \varphi^{\mathbf{k}}_{-}(z) = \begin{pmatrix} iA_3 S_z e^{-3i\phi_k} \\ A_2 C_z e^{-2i\phi_k} \\ iA_1 S_z e^{-i\phi_k} \\ A_0 C_z \end{pmatrix}, \tag{2.11}$$

where the wavevector $\mathbf{k} \perp \hat{z}$, $\phi_k$ is the angle between $\mathbf{k}$ and $\hat{x}$, $S_z = sin(q_h z) - (s_h/s_l) sin(q_l z)$, $C_z = cos(q_h z) - (c_h/c_l) cos(q_l z)$, where $s_h = sin(q_h d/2)$, $s_l = sin(q_l d/2)$, $c_h = cos(q_h d/2)$, $c_l = cos(q_l d/2)$. At $k \ll \pi/d$, the heavy and light hole ground state longitudinal wave vectors $q_h \sim \pi/d$ and $q_l = \sqrt{\nu} q_h$, $\nu = m_l/m_h$, $m_l$ and $m_h$ are light and heavy effective masses. Then in a spherical approximation the coefficients $A_0 = \sqrt{d/2}$, $A_1 = -\sqrt{3} k A_0/2q_h$, $A_2 = \sqrt{3} A_0 k^2/4q_h^2$, $A_3 = 3A_0 k^3/8\nu q_h^3$. Thus, two standing waves describe the 2D holes, reflecting their mutual transformation at interfaces, Fig.2.2.

Next we project the Hamiltonian of the system

$$H_h = H_L(\mathbf{K}) + H_1 + H_2 + U_v(z,\mathbf{r}) + \tilde{M}_{1z}J_z + \tilde{M}_{2z}J_z^3 \tag{2.12}$$

on the doublet $\varphi^{\mathbf{k}}_{+,-}(z,\mathbf{r})$. Here $U_v(z,\mathbf{r})$ is the potential confining holes including its asymmetric part, $\mathbf{K} = \mathbf{k} - \frac{e}{\hbar c}\mathbf{A}$, $\mathbf{A}$ is the vector-potential. Zeeman coupling of 2D holes to magnetic field $\mathbf{B} = curl\mathbf{A}$ comes from the orbital effect of magnetic field in the $(\hat{\mathbf{J}}\cdot\hat{\mathbf{p}})^2$ term of (2.5) and from pure Zeeman effects, $\tilde{M}_{1z} = \kappa\mu_B B$, $\tilde{M}_{2z} = q\mu_B B$, where $\kappa$ and $q$ are Luttinger parameters, and $\mu_B$ is the electron Bohr magneton. We consider $\mathbf{B}\|z$. The Dresselhaus coupling $H_1$ gives linear in $k$ 2D terms [22, 23, 42]

$$H_1 = \frac{1}{2}\delta\alpha_v \sum_j V_j p_j \left(p_j^2 - \frac{1}{3}p^2\right) - J_j^3\kappa_j \tag{2.13}$$

Here $V_z = J_xJ_zJ_x - J_yJ_zJ_y$, $\kappa_z = k_z(k_x^2 - k_y^2)$, and cyclic permutation of indices $x, y, z$ defines other $V_i$ and $\kappa_i$ components. The term $H_2$ in (2.12) is due to admixture of conduction electrons to holes,

$$H_2 = \zeta(\mathbf{J}\times\mathbf{p})\cdot\partial_{\mathbf{r}}U_e(z,\mathbf{r}), \tag{2.14}$$

where $U_e(z,\mathbf{r})$ is the potential acting on electrons, $\zeta = -P^2/3E_g^2$, $P$ is the Kane constant, $E_g$ is the band gap. Eq.( 2.14) gives $k^3$ 2D terms, which become linear in $k$ upon quantization in a 1D wire. In Eqs. (2.13, 2.14), we omit small terms $\propto J_i^3$ which are due to distant bands and result in much smaller spin-orbit coupling [22, 47, 48].

Our principal result is the effective 2D Hamiltonian

$$\begin{aligned}\mathcal{H} = {} & \tfrac{p^2}{2m} + V_{\mathbf{r}} + \tilde{\alpha}\sigma_z[\nabla_{\mathbf{r}}\tilde{V}_{\mathbf{r}}\times\mathbf{p}]_z + u(\sigma_x p_x + \sigma_y p_y) + \\ & \textstyle\sum_n \beta_n p^3(\sigma_x \sin n\phi - (n-2)\sigma_y\cos n\phi) + g\mu_B B\sigma_z,\end{aligned} \tag{2.15}$$

$n = 1, 3$. The effective 2D mass $m$ and $g-$factor are

$$\frac{m_0}{m} = \gamma_1 + \gamma_2 - 3a^2\gamma_2 + 3a^2(\gamma_1^2 - 4\gamma_2^2)^{1/2}f, \tag{2.16}$$

$$g = 6\kappa + \frac{27}{2}q - 6a^2\gamma_2 + 6a^2(\gamma_1^2 - 4\gamma_2^2)^{1/2}f, \tag{2.17}$$

$m_0$ is a free electron mass, $f = \cot\frac{\pi}{2}\sqrt{\frac{\gamma_1-2\gamma_2}{\gamma_1+2\gamma_2}}$, $a = \frac{\gamma_3}{\gamma_2}$. Two last terms in (2.17) emerge as off-diagonal terms $\hat{p_z}(p_x[J_zJ_x] + p_y[J_zJ_y])$ contribute to symmetric state

energy as $\propto p_- p_+ = p^2 + i(p_x p_y - p_y p_x)$, and give antisymmetric state energy $\propto p_+ p_- = p^2 - i(p_x p_y - p_y p_x)$. At $B \neq 0$, $i(p_x p_y - p_y p_x) \to \frac{\hbar e B}{c}$, making the two last terms in (2.17) twice those in (2.16). This simple picture confirms g-factor obtained using Landau quantization [23].

There are three spin-orbit terms in the ground state Hamiltonian (2.15). The Dresselhaus term is given by

$$u = \frac{1}{2}\left(\frac{\pi}{d}\right)^2 \delta\alpha_v \left[1 - a\left(1 - \sqrt{\nu}\frac{\gamma_1}{\gamma_2} f\right)\right], \tag{2.18}$$

where $a = \frac{\gamma_3}{\gamma_2}$. The Rashba term is defined by $\beta_1$, $\beta_3$:

$$\beta_n = \frac{3eFd^4}{4\hbar^3\pi^4}\left[A_n\left(\frac{4f/\sqrt{\nu}}{1-\nu} - \frac{3+\nu}{4\nu}\right) + \tilde{\zeta}_n\right]. \tag{2.19}$$

Here $A_n = a(a + n - 2)$, and the asymmetric part of the external electric field and doping potential $eFz$, $|z| < \frac{d}{2}$, is assumed equal for valence and conduction electrons. Distinct offset potentials, $U_c$ for electrons and $U_v$ for holes, give nonzero $\tilde{\zeta}_n = \pi^2\hbar\zeta(n - 1)(U_c - U_v)/(2d^2 U_v)$. For the ground state, $\beta_1$ and $\beta_3$ describe $p^3$ Rashba coupling. The newly predicted $\beta_1$ term has the symmetry of the first harmonics in $\mathbf{p}$. It affects the hole transport, e.g., weak antilocalization [49]. We note that the term $\propto A_n$ in (2.19) is due to the matrix element $\langle \pm | eFz | \mp \rangle$ and accounts for infinite number of perturbative terms of the same order. Calculation [50] included terms with just two excited states and contributed only to $\beta_3$.

The $\sigma_{\mathbf{z}}$-term in Eq. (2.15) results in 2D holes skew scattering, but our interest here is such term due to the wire confinement potential. The effective potentials in Eq. (2.15) that define 2D transport and spectra of wires are

$$\tilde{V}_{\mathbf{r}} = \frac{3}{2d}\int_{-d/2}^{d/2}\left[U_v(z,\mathbf{r})S_z^2 + \frac{\zeta\pi^2\hbar}{d^2}U_e(z,\mathbf{r})C_z^2\right]dz, \tag{2.20}$$

$V_{\mathbf{r}} = \frac{2}{d}\int_{-d/2}^{d/2} U_v(\mathbf{r},z)C_z^2 dz$, and the constant $\tilde{\alpha} = d^2/\pi^2\hbar$.

For hole wires, in which the wire width in x-direction $w \gg d$ [11, 39, 51, 52], the 1D Hamiltonian is

$$H_{1D} = \frac{p_y^2}{2m} + \alpha\sigma_z p_y + u\sigma_y p_y + \beta\sigma_x p_y + M_z\sigma_z. \tag{2.21}$$

Here $M_z = g\mu_B B/2$, $\beta = (\beta_1 + 3\beta_3)(\pi\hbar/w)^2$. We find $\alpha$ in a model with $U_{v,e}(z, \mathbf{r})$ being products of functions depending only on $z$ and only on $x$. We take hole and electron symmetric wire potential $U_v^{(s)}(x) = U_v^{(w)}\theta(x)$ and $U_e^{(s)}(x) = U_e^{(w)}\theta(x)$, correspondingly, with $\theta(x) = -1$ at $|x| < w/2$ and $\theta(x) = 0$ otherwise. In electric field $F_x$ acting on both electrons and holes, $\alpha = 3\zeta eF_x(1-U_e^{(w)}/U_v^{(w)})$. Offset-dependent $\alpha$ and $\beta_3$ and $\alpha$ independent of $\tilde{V}$ stem from the Ehrenfest theorem on vanishing average gradient of a potential in confined states. Thus, for the cleaved edge overgrowth wires $\alpha$ can be sizable, while for lithographically defined wires $\alpha = 0$.

A gap separates ground and excited states of an in-plane and $z-$direction quantization in a wire. Eq. (2.21) fully accounts for hole physics via the modified mass, g-factor and spin-orbit constants. For MBS, this electron-like Hamiltonian allows to use methods of [31, 53, 54].

## 2.4 Realization of Majorana zero modes

With the effective Hamiltonian Eq. (2.21), we are ready to discuss the conditions for realizing the Majorana zero modes.

After spin rotations around z and x axis, Eq. (2.21) becomes

$$H_{1D} = \frac{p^2}{2m} + \gamma\sigma_y p + M_z(cos\theta\sigma_z + sin\theta\sigma_y), \tag{2.22}$$

where index $y$ of p is dropped, $\gamma = \sqrt{\alpha^2 + \beta^2 + u^2}$ describes the spin-orbit coupling and $sin\theta = \frac{\alpha}{\sqrt{\alpha^2+\beta^2+u^2}}$ measures the alignment of the Zeeman and spin-orbit fields. The ground state wavefunctions of (2.22) are labeled + and -. The superconducting pairing arises due to the proximity effect [11, 55–60].

For ground band holes in the wire, the superconducting Hamiltonian is $H_{SC} = \int d\mathbf{r}\Delta e^{i\phi}\hat{c}_+^\dagger\hat{c}_-^\dagger + H.c.$, where $\hat{c}_\pm^\dagger$ are the creation operators adding holes to + and - states, and $\Delta e^{i\phi}$ is the pairing potential. The BdG Hamiltonian in the Nambu $\tau$-space reads:

$$\begin{aligned} H_{BdG} &= (\frac{p^2}{2m} - \mu + \gamma\sigma_y p)\tau_z + M_z(cos\theta\sigma_z + sin\theta\sigma_y) \\ &+ \Delta cos\phi\tau_x - \Delta sin\phi\tau_y. \end{aligned} \tag{2.23}$$

To show the existence of MBS, we prove that there is a non-degenerate solution at $E = 0$ of the BdG equation $H_{BdG}\Psi = E\Psi$ at the boundary of two regions which are topologically different [53]. Due to the particle-hole symmetry, this solution has the form $\Psi = (\psi, i\sigma_y\psi^*)$, $\psi$ is a two-spinor. We note that this form of solution is similar to the Majorana spinor in the chiral representation, Eq. (1.6). We have

$$[(\frac{p^2}{2m} - \mu + \gamma\sigma_y p) + M_z(cos\theta\sigma_z + sin\theta\sigma_y)]\psi \\ +\Delta e^{i\phi} i\sigma_y\psi^* = 0. \tag{2.24}$$

Writing $\psi = \psi_R + i\psi_I$, the Eq. (2.24) can be written as:

$$(\frac{p^2}{2m} - \mu + \gamma\sigma_y p + i\Delta cos\phi\sigma_y + M_z cos\theta\sigma_z)\psi_R + (M_z sin\theta + \Delta sin\phi) i\sigma_y\psi_I = 0$$
$$(\frac{p^2}{2m} - \mu + \gamma\sigma_y p - i\Delta cos\phi\sigma_y + M_z cos\theta\sigma_z)\psi_I + (-M_z sin\theta + \Delta sin\phi) i\sigma_y\psi_R = 0 \tag{2.25}$$

MBS should exist for any of the choices of the phase of the order parameter $\phi$, therefore we can choose $M_z sin\theta = -\lambda\Delta sin\phi$ to decouple one of $\psi_R$ or $\psi_I$, where $\lambda = \pm 1$. From Eq. (2.25), for the functions $\psi_R$ ($\lambda = 1$) or $\psi_I$ ($\lambda = -1$) we obtain:

$$\begin{pmatrix} \frac{p^2}{2m} - \mu + M_z cos\theta & \lambda\Delta cos\phi - i\gamma p \\ -\lambda\Delta cos\phi + i\gamma p & \frac{p^2}{2m} - \mu - M_z cos\theta \end{pmatrix} \psi_{R/I} = 0. \tag{2.26}$$

We note that the sign of the Zeeman term in the Eq. (59) of [53] should be +, not -, and equations for $\psi_I$ and $\psi_R$ cannot be both decoupled by a unique choice of $\phi$, but we can first obtain one of the $\psi_I$ and $\psi_R$, then using Eq. (2.25) to obtain the other one. The uniqueness of the solution will not be affected.

At $\psi_{I/R} \sim e^{-\tau y}$ a secular equation for $\tau$ is

$$\frac{\tau^4}{4m^2} + (\frac{\mu}{m} + \gamma^2)\tau^2 + 2\lambda\gamma\Delta cos\phi\tau + C_0 = 0, \tag{2.27}$$

where $C_0 = \mu^2 + \Delta^2 - M_z^2$. Using Vieta's formulas, for $C_0 < 0$ we find 3 roots with $Re[\tau] > 0$ and 1 root with $Re[\tau] < 0$ for $\lambda = -1$, or 1 root with $Re[\tau] > 0$ and 3 roots with $Re[\tau] < 0$ for $\lambda = 1$. For $C_0 > 0$ there are two roots with $Re[\tau] \lessgtr 0$. Due to one normalization and four boundary conditions, a unique bound state exists at the

boundary between the topological phase with $C_0 = \Delta^2 + \mu^2 - M_z^2 < 0$ and a trivial phase with $C_0 > 0$, [16, 21]. Once $\psi_{R/I}$ is found from Eq. (2.26) for a given $\phi$, $\psi_{I/R}$ can be found from Eq.(2.24) providing the other equation coupling $\psi_{R/I}$ and $\psi_{I/R}$. At $E = 0$ these $\psi_{I/R}$ define the wavefunction of the MBS. Hence the criterion for the topological superconductivity in hole wires is

$$M_z^2 > \mu^2 + \Delta^2. \tag{2.28}$$

Deriving (2.28) we used $M_z sin\theta = \pm\Delta sin\phi$. Therefore the existence of MBS for arbitrary $\phi$ requires

$$|\Delta| \geq |M_z sin\theta|. \tag{2.29}$$

A question is whether MBS exist when Eq. (2.24) cannot be decoupled. We show that for arbitrary $\phi$ the constraint $|\Delta| > |M_z sin\theta|$ is necessary for existence of a topological superconductor. If $sin\theta = 1$, i.e. the Zeeman and spin-orbit fields are aligned, MBS do not exist. If $sin\theta = 0$, they arise if Eq. (2.28) is satisfied. Furthermore, the MBS exist at $M_z sin\theta = \pm\Delta sin\phi$, for " intermediate" $\theta$. This precludes the possibility that only $sin\theta = 0$ case, i.e. when the BdG equations are equivalent to those with real coefficients, gives MBS, while other $\theta$ do not. Thus, a critical angle $\theta_c \neq 0$ exists when topological superconductivity emerges. Solving the BdG equation numerically for a quantum wire with open boundaries, we observe that the MBS exist only when both (2.28) and (2.29) are satisfied, and disappear when one of the conditions is not fullfilled. The results are summarized in Fig. 2.4. In Fig. 2.4(a), we found four zero modes in the spectrum, but only two of them are independent because the BdG formalism doubles the degree of freedom. These two independent zero modes correspond to two bound states located at the ends of the wire whose wave functions are plotted in the inset of Fig. 2.4(a). In the remaining three subfigures of Fig. 2.4, there are no zero modes in the spectrum and the wave functions do not localized at the ends of the wire. Therefore, Fig. 2.4 confirms that both (2.28) and (2.29) are required for the emergence of Majorana zero modes. Fig. 2.5 shows the ground state BdG energies for different $\Delta$ and $sin\theta$. We find that when $\Delta$ is too small (breaks

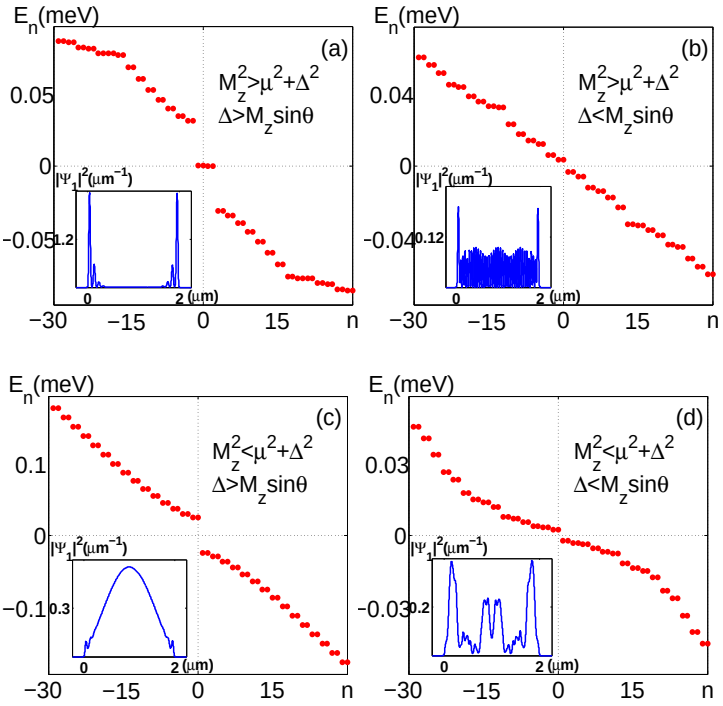


Figure 2.4. The BdG energy spectra $E_n$ in a 2 $\mu m$ long GaAs quantum wire. $B$ = 0.8$T$, $E_{so}$ = 0.2$meV$. a: $\mu$ = 0.5$M_z$,$\Delta$ = 0.6$M_z$, $sin\theta$ = 0. The zero energy solution exists and is well separated by a gap from the excited states. Inset: Majorana zero mode is localized at the boundary of the quantum wire. b,c,d: Parameters: b - $\mu$ = 0.5$M_z$,$\Delta$ = 0.6$M_z$, $sin\theta$ = 0.7; c - $\mu$ = 0.5$M_z$,$\Delta$ = $M_z$, $sin\theta$ = 0; d - $\mu$ = 0.9$M_z$,$\Delta$ = 0.6$M_z$, $sin\theta$ = 0.7. There are no zero energy solutions. Insets: Wavefunctions of the lowest-lying states. Majorana zero modes disappear in cases b,c,d.

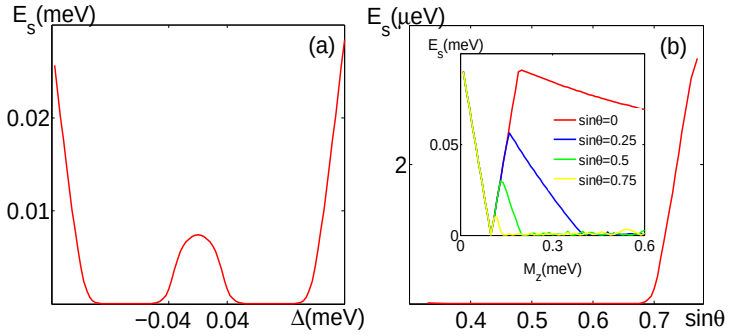


Figure 2.5. a: the BdG ground state energy $E_s$ for different $\Delta$. $M_z$ = $0.2meV$, $E_{so}$ = $0.2meV$, $\mu$ = $0.6M_z$ and $sin\theta$ = 0.2. $E_s \neq 0$ at $|\Delta| < 0.2M_z$ or $|\Delta| > 0.8M_z$, which correspond to $\Delta < M_z sin\theta$ and $M_z^2 < \mu^2 + \Delta^2$, respectively. b: $E_s$ for different $sin\theta$ ($\mu = 0.5M_z$, $\Delta = 0.7M_z$). $E_s$ is non-zero at $\Delta < M_z sin\theta$. Inset: Excitation gap versus $M_z$. $\Delta = 0.1meV$, $\mu = 0$. The gap closes at $M_z = \Delta$ or $\Delta/M_z = sin\theta$.

the condition Eq. (2.29) or too large (breaks the condition Eq. (2.28), there is no zero modes. We find that the critical angle for Eq. (2.29) is given by $\Delta = M_z sin\theta_c$ from Fig. 2.5. The extra constaint allows to control topological superconductivity tuning the $\sigma_z$-term by electrostatic gates at arbitrary direction of the magnetic field. In electron cases discussed in [16, 21, 53, 61], the constraint is on the direction of the magnetic field.

We find that hole wires in GaAs or InSb structures are favorable for MBS detection. In these systems a surface pinning of the Fermi level can be close to the valence band giving a small Schottki barrier for electrostatic control of charge carrier density. For $w = 80nm$ nanowire, lithographically developed from an unstrained $d = 20nm$ quantum well in a AlGaAs/GaAs/AlGaAs Carbon-doped heterostructure grown along [001], at $\gamma_1$ = 6.8, $\gamma_2$ = 2.1, $\gamma_3$ = 2.9, $\kappa$ = 1.2, $q$ = 0.04, $P = 10eV\mathring{A}$, $E_g = 1.52eV$ and [22] $\delta\alpha_v$ = 76.7 eV $\mathring{A}^3$, assuming $eF_z = 2 \times 10^4 V/cm$, we obtain $m$ = 0.15 $m_0$ ( $m = 0.25m_0$ when adjustments are made for the effects of finite depth of the well and one-sided doping), $g$ = 5, and $\gamma$ = 70 meV $\mathring{A}$. At 2D density $n_s = 2 \times 10^{10} cm^{-2}$, $\mu = 0.14meV$, and holes are only in the ground subband in the wire. For superconductivity caused by proximity to NbN, $\Delta \sim 0.1meV$, and the transition between topological and non-

topological superconducting order occurs at $B \sim 0.7T$. Then $E_{so} = 0.2meV > M_z$, and the lowest single-hole state is of camel-back type, Fig.2.1(a), i.e., spin-orbit coupling is strong.

For a similar InSb wire in InSb/AlInSb structure, at $\gamma_1 = 40.1$, $\gamma_2 = 18.1$, $\gamma_3 = 19.2$, $\kappa = 17.0$, $q = 0.5$, $P = 9.6eV\mathring{A}$, $E_g = 0.23eV$ and [47] $\delta\alpha_v = 70$ eV $\mathring{A}^3$, we get $\gamma \sim 250meV\text{Å}$, and $g \sim 90$. Due to strain in this system, $m = 0.04m_0$ [62] [according to Eq.(4.9) at zero strain, $m = 0.018m_0$]. Then $E_{so} \sim 0.4meV$. In proximity with NbN at $\Delta \sim 0.15meV$, $n_s = 2 \times 10^{10}cm^{-2}$, we find the transition between topological and non-topological superconductivity in the InSb hole wire at $B \sim 0.4T$. Then $M_z > E_{so}$, and the ground state of Eq.(2.22) has single-minimum Fig.2.1(b) shape, which is also the case in an electron InSb wire [55] with $E_{so}$ 4 times smaller than here.

## 2.5 Conclusion

In this chapter, I review the basic facts of band structure and spin orbit couplings of holes. I introduce our work of spin orbit couplings for low dimensional holes and emergence of Majorana zero modes. For the analysis of holes, we treat hole wires non-perturbatively, including the effect of mutual transformation of heavy and light holes at heteroboundaries, and derived the hole g-factor and spin-orbit interactions. For the analysis of Majorana zero modes, we find that Majorana settings in GaAs and InSb hole quantum-well–based wires exhibit considerably stronger p-type proximity-induced superconducting pairing compared to InSb electron system. For topological quantum computing, quantum-well–based wires could be of special importance because they may provide a natural path for construction of networks of high-mobility wires for braiding Majorana modes. We discuss a criterion for transition from non-topological to topological superconducting order, showing that Majorana modes arise even if the Bogoliubov-De Gennes equations for real and imaginary parts of the wave-function cannot be decoupled. We also show that an extra constraint is necessary for appearance of Majorana zero modes. Beyond Majorana context, our results are

important for the field of spin-based electronics, for generation, manipulation and transmission of spin currents.

# 3. INTRODUCTION TO PARAFERMIONS AND QUANTUM HALL EFFECT

Although the Majorana fermion is an important step towards topological quantum computation, it is not computationally universal [63,64]. Braiding Majorana fermions can not produce all unitary quantum gates, such as the entangling gate [64,65]. This fact forces us to search for more powerful non-Abelian anyons. The parafermion is a promising candidate. The braiding statistics of parafermions is richer than Majorana fermions [64]. Furthermore, they present a vital step toward the realization of Fibonacci anyons that allow a full set of quantum operations with topologically protected quasiparticles [66]. However, the emergence of parafermions requires strong electron-electron interactions. Fractional quantum Hall systems are studied by many authors and are expected to be grounds for realizations of abelian anyons and non-Abelian anyons [8, 13, 64, 67–69]. Therefore, we also study parafermions in the fractional quantum Hall regime. Before introducing our work, in this chapter I will give an introduction to the quantum Hall effect and its edge theory which are essential for the study of parafermions. I will also overview the basic properties of parafermions.

## 3.1 Integral Quantum Hall Effect

The integral quantum Hall effect was discovered by von Klitzing and coauthors in 1980 [70]. This beautiful discovery opens a new era of condensed matter physics. A schematic plot of the experimental setting is given by Fig. 3.1. The Hall resistance is defined by $R_H = \frac{V_H}{I}$. The longitudinal resistance is given by $R_L = \frac{V_L}{I}$. Two main results of the integral quantum Hall effect can be summarized as below [71]:
(1)Quantization of resistance. When the Hall resistance $R_H$ is plotted as a function

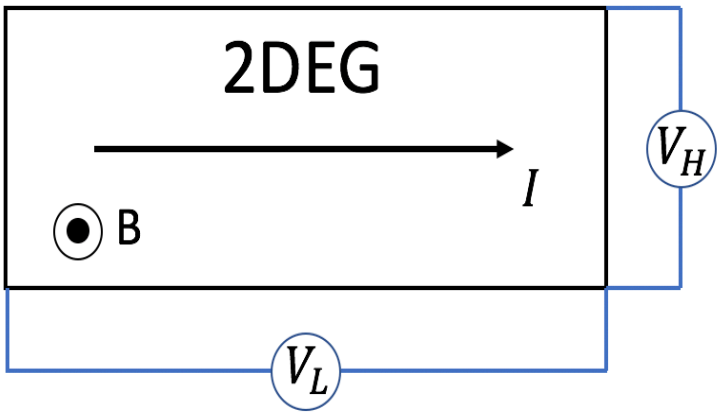


Figure 3.1. A schematic plot of magnetotransport measurement. A strong magnetic field is applied perpendicular to the two dimensional electron gas(2DEG). $V_L$, $V_H$ and $I$ are longitudinal voltage, Hall voltage and current, respectively.

of the magnetic field B, it shows many plateaus. The plateaus happen approximately when the electrons fill integer Landau levels $n$. The Hall resistance is given by:

$$R_H = \frac{h}{ne^2} \tag{3.1}$$

where $h$ is the Planck constant and $e$ the electron charge.

(2)Superflow. When $R_H$ is in the plateau regions, the $R_L$ shows Arrhenius behavior:

$$R_L = exp(-\frac{E_g}{2k_BT}) \tag{3.2}$$

The $E_g$ can be interpreted as an energy gap in the spectrum. We note that when the temperature $T$ goes to zero, the $R_L$ also goes to zero which means the electrons travel without dissipation.

To understand the nature of the quantum Hall effect, we have to first understand the behavior of a single electron in the magnetic field in dimension two. The Hamiltonian that describes such an electron is:

$$H = \frac{1}{m_b}(\mathbf{p} + \frac{e\mathbf{A}}{c})^2 \tag{3.3}$$

The electron's charge is $-e$ and it is in the x-y plane. The vector potential $\mathbf{A}$ gives a magnetic field along z direction, $\nabla \times \mathbf{A} = B\hat{z}$. Denote the length along x and y

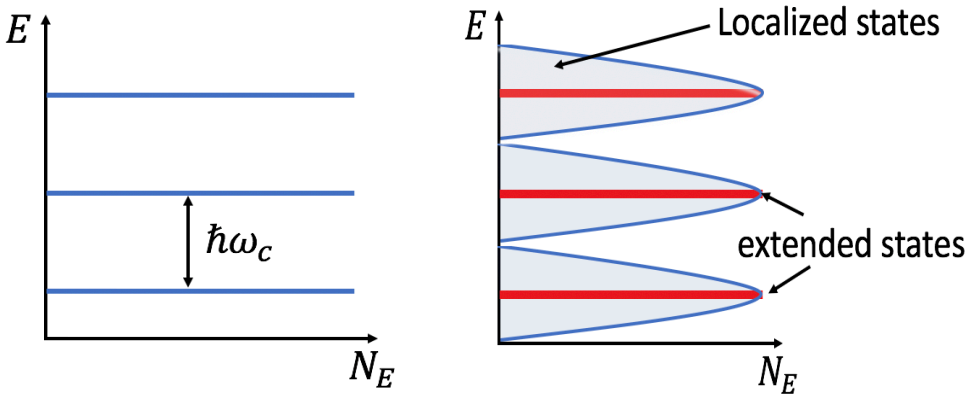


(a) (b)

Figure 3.2. a: a schematic plot of the Landau levels. $N_E$ is the electron density . b: The broadened Landau levels due the existence of impurity. The red regions denote the extended states that contribute to the transport, while blue shadow regions denote the localized states.

directions as $L_x$ and $L_y$, the magnetic length $l = \sqrt{\frac{\hbar c}{eB}}$ and the cyclotron frequency $\omega_c = \frac{eB}{m_b c}$. For the Landau gauge $\mathbf{A} = -Bx\hat{y}$, the energy eigenvalues of Eq. (3.3) are given by

$$E_n = (n + \frac{1}{2})\hbar\omega_c \tag{3.4}$$

with $n = 0, 1, ..., \infty$. These discrete energy levels are called Landau levels and the gap between two neighboring Landau levels is $\hbar\omega_c$, see Fig. 3.2(a). The wave functions in the $n^{th}$ Landau level are [72]:

$$\psi_n(x,y) = \frac{1}{\sqrt{2^n n! \pi^{\frac{1}{2}} l L_y}} e^{ik_y y} e^{-\frac{(x-k_y l^2)^2}{2l^2}} H_n(\frac{x - k_y l^2}{l}) \tag{3.5}$$

where $H_n(x)$ is the Hermite polynomial of order n. From the above expression, we see that each Landau level is highly degenerate. The degeneracy per unit area is:

$$D = \frac{1}{2\pi l^2} = \frac{B}{\phi_0} \tag{3.6}$$

where $\phi_0 = hc/e$ is the flux quantum.

It is also very useful to work out the solution in the symmetric gauge: $\mathbf{A} = \frac{1}{2}\mathbf{B}\times\mathbf{r}$. The energy levels are given by:

$$E_n = (n+\frac{1}{2})\hbar\omega_c = (n_r + \frac{|m|-m}{2} + \frac{1}{2})\hbar\omega_c \tag{3.7}$$

where both $n$ and $n_r$ are non-negative integers and we have $m \geqslant -n$. The wave functions are:

$$\psi_{n_r,m}(r,\phi) = \frac{1}{l}\sqrt{\frac{n_r!}{(n_r+|m|)!}}(\frac{r}{\sqrt{2}l})^{|m|}e^{-\frac{r^2}{4l^2}}L_{n_r}^{|m|}(\frac{r^2}{2l^2})e^{im\phi} \tag{3.8}$$

where $L_n^{|m|}$ are the associated Laguerre polynomials. Although the above expression seems complicated, it has a very useful property in the lowest Landau level (LLL), the analyticity. The wave functions in the LLL:

$$\psi_{0,m} \equiv \psi_m(z) = \frac{1}{\sqrt{2\pi l^2 2^m m!}} z^m e^{-\frac{|z|^2}{4l^2}} \tag{3.9}$$

Therefore, the N-electron wave function which lies entirely in the LLL takes the form:

$$f(z_1,...,z_N)\prod_{i=1}^{N} e^{-\frac{|z_i|^2}{4l^2}} \tag{3.10}$$

where $f(z_1,...,z_N)$ is an analytic function for all arguments $z_1$, ..., $z_N$. This property is very important for analyzing the fractional quantum Hall effect where all the electrons reside in the LLL.

The Landau level picture in Fig. 3.2(a) can not explain the quantum Hall plateaus. We need the concepts of extended states and localized states. After including the effects of impurities, many states appear in the gaps between the Landau levels. The Landau levels broaden into bands, see Fig. 3.2(b). However, these states represent close orbits of electrons, so they are localized states that do not contribute to the transport. The blue shadow regions in Fig. 3.2(b) denote these states. In addition, at the edges of the sample, electrons feel a steep potential. These edge states go across the entire length of the sample, thus they are extended states that contribute to the transport. The energies of these edge states are near the center of Landau levels, which are represented by red regions in Fig. 3.2(b). The origin of the plateaus

can be explained like this: We start from filling factor n, so the electrons fill n Landau levels with Hall resistance $R_H = h/ne^2$. Now we add more electrons into the system and the filling factor goes away from n. However, these extra electrons just occupy the localized states and they do not contribute to transport. Therefore, the Hall resistance is still given by $R_H = h/ne^2$. If we change the magnetic field, we basically change the degeneracy of the Landau levels, Eq. (3.6), and it's equivalent to add or subtract electrons to the system. The Hall resistance remains a constant, so a plateau is observed. One may argue that the Hall resistance is given by $R_H = \frac{B}{\rho_{ex}ec}$, with $\rho_{ex}$ the density for extended states. However, a careful calculation shows that $R_H = \frac{B}{\rho ec}$ as if all the electrons contribute to the transport [71].

## 3.2 Fractional Quantum Hall Effect

In 1982, Tsui and his coauthors observed the Hall resistance plateaus at $R_H = \frac{h}{\nu e^2}$ where $\nu$ is a rational number [73]. The first observed $\nu$ is $\frac{1}{3}$. This result is surprising, since according to our analysis in the last section, there is no gap within the lowest Landau level (LLL). The kinetic part of the electron motion, governed by Eq. (3.3), is a constant in the LLL. Therefore, electron-electron interaction plays an important role:

$$H_{in} = \sum_{i<j} \frac{e^2}{\epsilon |r_i - r_j|} \tag{3.11}$$

The interaction term Eq. (3.11) can not be treated using mean field theories [71]. We have to use new methods to explain the fractional quantum Hall effect. There are three important ways to understand the nature of the fractional quantum Hall states:

(1) The Laughlin wave function. In low temperature, the behaviors of a gapped system are mostly determined by the ground state wave function. Laughlin is the first one to put forward a trial wave function as the ground state for fractional quantum

Hall effect at filling factor $\nu = \frac{1}{3}$ [74]. His method is generalized to $\nu = \frac{1}{m}$ with $m$ an arbitrary odd number. For $\nu = \frac{1}{m}$, the Laughlin wave function for N electrons is:

$$\Psi_m(z_1, ..., z_N) = \prod_{i<j}^{N}(z_i - z_j)^m \prod_{i=1}^{N} e^{-\frac{|z_i|^2}{4l^2}} \tag{3.12}$$

where $z_k = x_k + iy_k$ denotes the position of kth electron in the plane and $l$ is the magnetic length. It is verified that the Laughlin wave function is a valid and accurate representation of the true ground states at filling fraction $\nu = 1/3$ and $\nu = 1/5$ [71]. Starting from the Laughlin states, we can also construct excitations by attaching flux tubes. The quasihole excitation at position $z_0$ is given by:

$$\Psi_m^{h,z_0}(z_1, ..., z_N) = \prod_i (z_i - z_0) \prod_{i<j}^{N}(z_i - z_j)^m \prod_{i=1}^{N} e^{-\frac{|z_i|^2}{4l^2}} \tag{3.13}$$

The quasiparticle excitation at position $z = z_0$ is given by:

$$\Psi_m^{e,z_0}(z_1, ..., z_N) = \prod_{i=1}^{N} e^{-\frac{|z_i|^2}{4l^2}} (2\frac{\partial}{\partial z_i} - \frac{z_0^*}{l^2}) \prod_{i<j}^{N}(z_i - z_j)^m \tag{3.14}$$

These quasihole and quasiparticle excitations have two very interesting and important properties: fractional charge and fractional statistics. The fractional charge of the quasihole can be seen in the following way: The radius of the electron liquid of Laughlin state is given by $r_0 = l\sqrt{2m(N-1)}$, while the radius of the quasihole state is $r_h = l\sqrt{2m(N-1)+1}$. The extra charge is given by

$$q_h = e\rho\pi(r_h^2 - r_0^2) = \frac{e}{m} \tag{3.15}$$

Therefore, we can effectively view the quasihole as if it carries charge $e/m$. The exchange statistics of two quasiholes can be obtained by calculating the Berry phase: $\gamma = i \oint dz_0 \langle \Psi_m^{h,z_0} | \frac{d\Psi_m^{h,z_0}}{dz_0} \rangle$. For the $\nu = 1/3$ Laughlin state, the exchange phase of quasiholes is $e^{i\pi/3}$ [72].

(2)Composite fermions. The Laughlin wave functions only solve the problem at filling factor $\nu = 1/m$, so we need to use new methods to explain the more complicated filling factors such as 2/5, 2/7, and so on. The composite fermion theory is an effective way to obtain the ground state wave functions for a large set of filling

factors. A composite fermion is the bound state of an electron and an even number of quantized vortices. By transforming the electrons into composite fermions, one can build correspondences between the fractional quantum Hall states and integral quantum Hall states. We can see how it works in the following:

We start from an integer quantum Hall state at filling factor $n$ which is an integer. The spectrum has gaps. The relation between the density $\rho$ and the applied magnetic field is $\rho = \frac{n|B_0|}{\phi_0}$, where $\phi_0 = hc/e$ is the flux quanta. $B_0$ is positive when it is along $+z$ direction. Now we attach $2p$ flux quanta to each electron, the new magnetic field is given by:

$$B = B_0 + 2p\phi_0\rho \tag{3.16}$$

The new filling factor is $\nu$ and $\rho = \frac{\nu B}{\phi_0}$. Substituting this relation and $\rho = \frac{\pm nB_0}{\phi_0}$ into Eq. (3.16), we have

$$\nu = \frac{n}{2pn \pm 1} \tag{3.17}$$

Therefore, the fractional quantum Hall effect of electrons can be regarded as integer quantum Hall effect of composite fermions. The important point is, during the flux attaching process, the gap in the integer filling factor $n$ persists to the fractional filling factor $\nu = \frac{n}{2pn\pm1}$. The explanations for the integral effect can be applied similarly to explain the fractional effect. Furthermore, the composite fermion theory allows us to construct the ground state wave function for filling factor $\nu = \frac{n}{2pn\pm1}$. To see this, we first find out the vector potential that binds $2p$ flux quanta to electrons. It is given by [71]:

$$\mathbf{A}_{2p}(z_i) = \frac{2p}{2\pi}\phi_0 \sum_{j\neq i} \nabla_i \theta_{ij} \tag{3.18}$$

with

$$\theta_{jk} = i\ln\frac{z_j - z_k}{|z_j - z_k|} \tag{3.19}$$

This vector potential can be eliminated by making gauge transformation, thus the wave function should have a phase factor:

$$e^{-2ip\sum_{j<k}\theta_{jk}} = \prod_{j<k}\left(\frac{z_j - z_k}{|z_j - z_k|}\right)^{2p} \tag{3.20}$$

By considering the correlations between electrons and the Landau levels mixing, the proposed wave function for filling factor $\nu = \frac{n}{2pn\pm1}$ is given by [71]:

$$\Psi_\nu = \mathcal{P}_{LLL}\Phi_{\pm n}\prod_{j<k}(z_j - z_k)^{2p} \tag{3.21}$$

where $\mathcal{P}_{LLL}$ is the projection operator into lowest Landau levels and $\Phi_{\pm n}$ is the wave function for filling full $n$ Landau levels.

(3)Effective field theory. The effective field theory is a phenomenological theory proposed by Wen to describe the fractional quantum Hall states [13,75,76]. It can reproduce the basic results of these states such as fractional charge, fractional statistics, and so on. Furthermore, it is useful for analyzing the edge states and the interplay of fractional quantum Hall effect and other phenomena such as superconductivity and tunneling. Here I summarize the basic results of this theory.

The number and current density of the electron is represented by $J(z) = (J^0(z), \mathbf{J}(z))$, with $J^0$ the number density. We set $\hbar = c = 1$. The basic relations of the quantum Hall effect is given by

$$\begin{aligned} J^0 &= \frac{-e\nu B}{2\pi} \\ \sigma_{xy} &= \frac{\nu e^2}{2\pi} \\ J^x &= \sigma_{xy}E^y \end{aligned} \tag{3.22}$$

It can be written in a compact way:

$$eJ^\mu = \frac{\nu e^2}{2\pi}\epsilon^{\mu\nu\lambda}\partial_\nu A_\lambda \tag{3.23}$$

The next step is to find out a Lagrangian which produce an equation of motion like Eq. (3.23). Introducing a U(1) gauge field $a_\mu$ to describe the densities: $J^\mu = \frac{1}{2\pi}\partial_\nu a_\lambda \epsilon^{\mu\nu\lambda}$. The Lagrangian that produces Eq. (3.23) for Laughlin states $\nu = 1/m$ is given by [13]:

$$L = -\frac{m}{4\pi}a_\mu\partial_\nu a_\lambda\epsilon^{\mu\nu\lambda} + \frac{e}{2\pi}A_\mu\partial_\nu a_\lambda\epsilon^{\mu\nu\lambda} \tag{3.24}$$

The fractional charge and fractional statistics can be explained using the effective field theory. Let us create a particle with $a_\mu$ charge l. It is equivalent to adding a

source term $la_0\delta(z-z_0)$ into Eq. (3.24). The equation of motion with respect to $a_0$ gives:

$$J_0 = \frac{1}{2\pi}\epsilon_{ij}\partial_i a_j = -\frac{e}{2\pi m}B + \frac{l}{m}\delta(z-z_0) \tag{3.25}$$

Therefore, one $a_\mu$ charge carries $\frac{e}{m}$ electric charge. From Eq. (3.25), one can see that the source term also create $\frac{l}{m}$units of $a_\mu$ flux. Exchange two excitations induce a phase [13]:

$$\theta = \pi\frac{l^2}{m} \tag{3.26}$$

A general fractional quantum Hall state at filling fraction $\nu$ can be regarded as consisting of several condensates and the $I^{th}$ condensate is determined by a gauge field $a_{I\mu}$. The Lagrangian describes such a general fractional quantum Hall state is [76]:

$$L = -\frac{1}{4\pi}K_{IJ}a_{I\mu}\partial_\nu a_{J\lambda}\epsilon^{\mu\nu\lambda} + \frac{e}{2\pi}q_I A_\mu\partial_\nu a_{I\lambda}\epsilon^{\mu\nu\lambda} + s_I\omega_\mu\partial_\nu a_{I\lambda}\epsilon^{\mu\nu\lambda} \tag{3.27}$$

where the matrix $K$ describes the couplings between different condensates, the charge vector $q$ describes the couplings between electro-magnetic field and the condensates, and spin vector $s$ describes the couplings between curvature and the condensates. The spin vector appears because of the shift $S$ for a quantum Hall state on a curved surface:

$$N_\phi = \nu^{-1}N_e - S \tag{3.28}$$

where $N_\phi$ is the total number of flux quantum passing through the surface, $N_e$ is the Landau level degeneracy. $S$ depends on the Landau level index and the topology of the space. For $\nu = 1$ state, $S = 1$ for sphere and $S = 0$ for torus. Therefore, to describe this effect, we need the third term in the Lagrangian Eq. (3.27). The set ($K$, $q$, $s$) characterizes the topological order of a quantum Hall state. The filling fraction is given by [13]:

$$\nu = \mathbf{q}K^{-1}\mathbf{q} \tag{3.29}$$

For a quasiparticle labeled by $\mathbf{l}$ which has $l_I$ charge in the $I^{th}$ component, the charge and statistics is given by [13]:

$$\begin{aligned} Q_l &= -e\mathbf{l}^\top K^{-1}\mathbf{q} \\ \theta_l &= \pi\mathbf{l}^\top K^{-1}\mathbf{l} \end{aligned} \tag{3.30}$$

### 3.3 Edge Physics of Quantum Hall States

In the single-electron picture, the edge states refer to the quantum states which are localized around the edge of the system. For the electron liquids, the edge states can be roughly regarded as surface waves or surface fluctuations of the electron droplets. In the quantum Hall regime, edge states normally represent the low-lying gapless excitations of the systems. These low-lying states are important for the electron transport. However, due to the competition between the Coulomb interaction and the sharp edge confinement potential, the structure of the edge may be very complicated [77–80]. The edge density may not fall from the bulk density directly to zero. Edge reconstructions may happen and more conducting channels form around the edge. For example, the possible edge structure of $\frac{2}{3}$ state is plotted schematically in Fig. 3.3. For the sharp clean edge, a $\nu = 1$ state may form [77] and we will have two counter-propagating edge modes, see Fig. 3.3(a). For the smooth edge and the existence of disorder, some other incompressible states may form and its behaviors may be very complicated [80], see see Fig. 3.3(b).

There are basically three ways to study the edge structure: numerical calculations, constructions of wave functions and the effective field theory. For numerical calculations, we exactly diagonalize the Hamiltonian of the electron system with the confinement potential. The low-lying energy edge states can be obtained from the spectrum of the Hamiltonian. Then the density profiles of these edge states can be obtained from the wave functions and the edge structures can be studied.

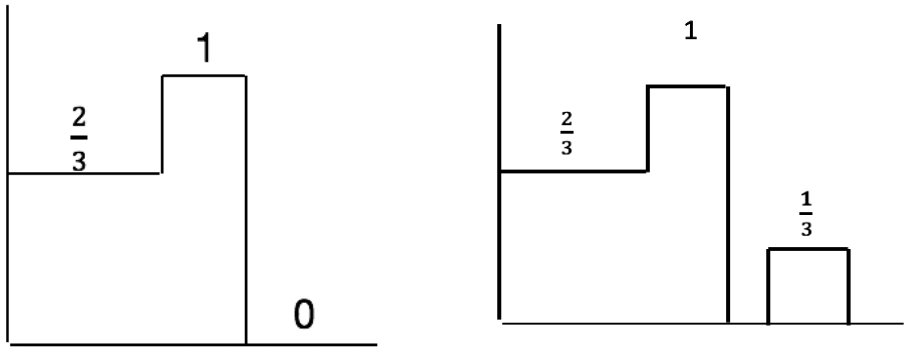


(a) (b)

Figure 3.3. Schematic plots of the edge structure of the spin-polarized 2/3 state. a: For the sharp clean edge confinement, a $\nu = 1$ state may form around the edge [77]; b: For the smooth edge confinement and with disorder, a $\nu = 1/3$ state or other incompressible states may form [80].

To construct the wave functions of the edge states, one needs to know the ground state wave function. For the Laughlin state $\Phi_3(z) = \prod_{i<j}(z_i - z_j)^3$, the following states all represent the low lying states [13]:

$$\Phi_{edge}(z) = F(z)\Phi_3(z) \tag{3.31}$$

where $F(z)$ is a symmetric polynomial. One can check the validity of the above assertion by numerical calculations. From this result, we see that the quasihole and quasiparticle excitations can all be regarded as edge states. For more general filling fractions, one can construct the edge states by multiplying the ground state wave functions with Schur functions [81].

As the edge states are localized around the edge, their effective theory should be an one spacial dimension theory. Wen found out that these edge states are described by the so called "chiral Luttinger liquid", which is different from the normal Luttinger liquid since the edge modes here propagate only in one direction [82]. According to Ref. [13], I summarize the basic results of this theory as below.

We associate one edge effective field $\phi_I$ to each bulk gauge field $a_{I\mu}$. The edge density of the Ith condensate of the fractional quantum Hall state is given by:

$$\rho_I = \frac{1}{2\pi}\partial_x \phi_I \tag{3.32}$$

The edge densities obey the Kac-Moody (K-M) algebra:

$$\begin{aligned} [\rho_{Ik}, \rho_{Jk'}] &= (K^{-1})_{IJ}\frac{1}{2\pi}k\delta_{k+k'} \\ k, k &= integer \times \frac{2\pi}{L} \end{aligned} \tag{3.33}$$

where the K matrix is the same as the bulk effective theory. The Hamiltonian is given by:

$$H = 2\pi \sum_{IJ} V_{IJ}\rho_{I,-k}\rho_{J,k} \tag{3.34}$$

The quasiparticle operators $\Psi_l \propto e^{i\phi_I l_I}$ creates charge:

$$Q_l = -e\mathbf{q}^\top K^{-1}\mathbf{l} \tag{3.35}$$

From the above expression, it is obvious that an electron operator should satisfies:

$$l_I = K_{IJ} L_J, \quad q_I L_I = 1 \tag{3.36}$$

The mathematical structure of these edge modes are very useful when we study their couplings to the superconductors.

### 3.4 Parafermions

As I mentioned before, the Majorana fermion alone can not be used to perform universal topological quantum computation since the lack of entangling quantum gates. In this section, I will introduce some important properties of parafermions, based on the work in Ref. [64, 83].

Let us consider the generalized N-state quantum clock model:

$$H = -J \sum_{j=1}^{L-1} (\sigma_j^\dagger \sigma_{j+1} + \sigma_{j+1}^\dagger \sigma_j) - h \sum_{j=1}^{L} (\tau_j^\dagger + \tau_j) \tag{3.37}$$

where the $\sigma$ and $\tau$ are unitary operators that satisfy $\sigma_j^N = \tau_j^N = 1$. The only non zero commutation relation is given by:

$$\sigma_j \tau_j = \tau_j \sigma_j e^{2\pi i/N} \tag{3.38}$$

We can define a new set of operators $\alpha_j$ by the following transformation:

$$\begin{aligned} \alpha_{2j-1} &= \sigma_j \prod_{i<j} \tau_i \\ \alpha_{2j} &= -e^{i\pi/N} \tau_j \sigma_j \prod_{i<j} \tau_i \end{aligned} \tag{3.39}$$

These new operators have the following properties:

$$\begin{aligned} \alpha_j^N &= 1 \\ \alpha_j^\dagger &= \alpha_j^{N-1} \\ \alpha_j \alpha_k &= \alpha_k \alpha_j e^{\frac{2\pi i}{N} sgn(k-j)} \end{aligned} \tag{3.40}$$

For $N = 2$ case, these operators represent Majorana fermions. For $N > 2$, they define the parafermions. In terms of these new operators, the Hamiltonian in Eq. (3.37) becomes:

$$H = J\sum_{j=1}^{L-1}(e^{-i\pi/N}\alpha_{2j}^{\dagger}\alpha_{2j+1} + h.c.) + h\sum_{j=1}^{L}(e^{i\pi/N}\alpha_{2j-1}^{\dagger}\alpha_{2j} + h.c.) \tag{3.41}$$

The structure of this Hamiltonian is similar to Fig. 1.1. When $J = 0$, all the parafermions are paired. While for $h = 0$, we have two unpaired parafermion operators. One can show that a pair of parafermion operators define an N dimensional Hilbert space. Let us take the two operators as $\alpha_1$ and $\alpha_2$. We first observe that:

$$(\alpha_1^{\dagger}\alpha_2)^N = e^{i\pi(N-1)} \tag{3.42}$$

Therefore, the eigenvalues of $\alpha_1^{\dagger}\alpha_2$ have the form $-e^{\frac{2\pi i}{N}(q-1/2)}$ and the corresponding eigenvectors are $|q\rangle$, with $q$ takes the values 1, ...., N. Using the relations in Eq. (3.40), we see that $\alpha_1$ and $\alpha_2$ decrease the quantum number q by 1, while $\alpha_1^{\dagger}$ and $\alpha_2^{\dagger}$ increase q by 1. We also see that by applying $\alpha_1$ and $\alpha_2$ to $|q\rangle$, there is only a unique state $|q-1\rangle$. The reason is:

$$\alpha_2|q\rangle = \alpha_1\alpha_1^{\dagger}\alpha_2|q\rangle = q\alpha_1|q\rangle \tag{3.43}$$

Using the similar method, one can prove that all the states $|q\rangle$ are non-degenerate in the space defined by $\alpha_1$ and $\alpha_2$. With this result, we find that for $J = 0$ and $h \neq 0$, there is a unique gapped ground state. However, for $h = 0$, we have N degenerate ground states defined by $\alpha_1$ and $\alpha_{2L}$. These parafermionic zero modes can be used as topologically protected qubits.

The fractional quantum Hall state in proximity to the s-wave superconductors is proposed to host parafermion zero modes [64]. The fractional Josephson effect can be used to confirm the appearance of parafermions. For the Laughlin state $\nu = 1/m$, the Josephson current admits $4\pi m$ periodicity.

Braiding the parafermions can achieve entangling gates. Let us consider the state $|q, q'\rangle$ defined by two pairs of parafermions $\alpha_1$, $\alpha_2$, $\alpha_3$ and $\alpha_4$. $U_{ij}$ denotes a clockwise

exchange of $\alpha_i$ and $\alpha_i$. The operator $P = (U_{23}U_{12}U_{34}U_{23})^2$ produces a controlled phase gate. It yields:

$$P|q, q'\rangle = e^{-i(2\pi/m)(q-k-m)(q'-k-m)}|q, q'\rangle \tag{3.44}$$

From the above expression, we can see that the Majorana fermions with $m = 1$ can not produce such a gate.

# 4. PARAFERMIONS IN THE FRACTIONAL QUANTUM HALL SPIN TRANSITIONS

In this chapter, I will introduce our work about a possible setup that can host parafermions. We prove, by both analytical and numerical methods, that two counter propagating edge modes exist at the boundary between 2/3 spin polarized and unpolarized fractional quantum Hall states. Our field theory analysis and numerical calculation show that when these edge modes are coupled to superconductivity and subject to an in-plane magnetic field, parafermion zero modes can emerge. Some of the results of edge states in this chapter is published in Ref. [84].

## 4.1 Introduction

As reviewed in the first two chapters of the thesis, topological quantum computation using Majorana fermion based systems are studied by many authors [2, 9, 16, 28]. However, it is shown that such systems are not computationally universal since the braiding operations of Majorana fermions cannot approximate all unitary quantum gates [63, 85]. To realize universal topological quantum computation, we have to look for other kinds of non-Abelian anyons. The parafermion is such a candidate because it is shown to have denser rotation groups and its braiding operations enable two-qubit entangling gates [83, 86]. Furthermore, a two dimensional array of parafermions can support Fibonacci anyons with universal braiding statistics [66]. Therefore, the next step is to find out experimentally realizable systems which can host parafermions. In a seminal paper [64], Clarke *et al* proposed that parafermions can appear in the fractional quantum Hall effect regime if two counter-propagating edge states with different polarizations can be gapped by proximity superconducting pairing and tunneling. Here we suggest that the edge states formed during the spin transition of $\frac{2}{3}$

spin singlet state and spin polarized state can host parafermions when coupled to an s-wave superconductor.

The spin transitions of fractional quantum hall effect (FQHE) regime have been observed at the filling factor $\nu = \frac{2}{3}$ and other fractions [87, 88]. It is shown that using electrostatic gates that make exchange interactions in a system position-dependent, it is possible to have both polarized and unpolarized state in a single sample with a domain wall separating regions with different spin polarization [89, 90]. The spin transition can be understood in terms of the composite fermion (CF) picture. The FQHE states at filling fraction $\nu = \frac{n}{2n-1}$ can be mapped onto integer quantum Hall states at filling fraction $n$ for CFs. The energy of the nth level can be written as the following [84]:

$$E_{ns} = \hbar\omega_c^{cf}(n + \frac{1}{2}) + sg\mu_B B \tag{4.1}$$

Where $\hbar\omega_c^{cf}$ is proportional to $\frac{e^2}{\sqrt{l_m^2+z_0^2}}$ and $l_m \propto \sqrt{B_\perp}$ is the magnetic length with $B_\perp$ the out of plane component of magnetic field $B$, and $z_0$ is the extent of the wavefunction in the out of plane direction. The second term is the Zeeman energy and $s = \pm 1$ represent the spin. Since these two terms have different spin dependences, the levels $\Lambda_{p,\downarrow}$ and $\Lambda_{p+1,\uparrow}$ cross at some $B^* > 0$, as shown in Fig.4.1(a). Therefore, at $B < B^*$ electrons of $\frac{2}{3}$ state occupy $\Lambda_{0\uparrow}$ and $\Lambda_{0\downarrow}$ and it's in spin unpolarized state, while at $B > B^*$ they occupy $\Lambda_{0\uparrow}$ and $\Lambda_{1\uparrow}$ and it's in spin polarized state. Experimentally we can also tune the effective Coulomb interaction instead of tuning the Zeeman coupling to make the transition between spin polarized and unpolarized state [84].

In this chapter we will study the edge state structure on the boundary of the $\frac{2}{3}$ polarized and unpolarized state. The edge states of the quantum Hall systems are widely studied over years [75–78, 91–93]. For the filling fraction $\frac{2}{3}$, edge states between fractional quantum Hall liquid and the vacuum have been studied in both spin polarized and various kind of unpolarized phases [80, 81, 94, 95]. It is anticipated that both phases of $\frac{2}{3}$ have two edge modes moving in different directions for clean edges [75, 77]. When the $\frac{2}{3}$ polarized and unpolarized states are far apart, there are four edge modes with two moving right and two moving left. When they are attached

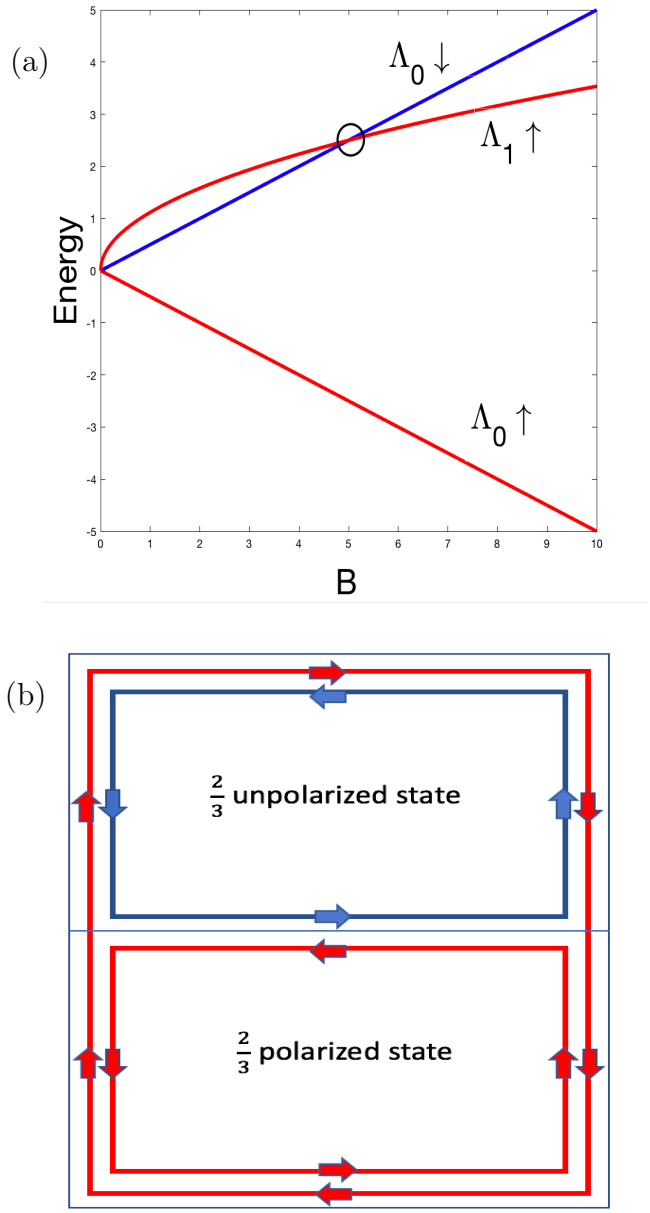


Figure 4.1. a: The schematic plot of the composite fermion energy levels. When the magnetic field is increased, there is a level crossing(black circle) of the $\Lambda_{0\downarrow}$ and $\Lambda_{1\uparrow}$ which leads to a spin transition from spin singlet state to spin polarized state. b: A schematic plot of the edge states. The arrows represent the direction of the their velocities and colors represent spin up(red) spin down(blue).

together, we anticipate that there are only two edge modes left, see Fig.4.1(b). This can be understood intuitively in terms of the CF picture. The edge states associated with the common $\Lambda_{0\uparrow}$ level will merge and disappear so only the edges states associated with the $\Lambda_{0\downarrow}$ and $\Lambda_{1\uparrow}$ levels exist. This picture also indicates that the remaining edge states should propagate in different directions and carry different spins.

In the following of this chapter, we will first use the effective theory to show that the above picture is true. We will also apply exact diagonalization method to the Hamiltonian of disk and torus geometies and prove that there are indeed two counter-propagating edge modes with different spin polarizations at the boundaries between spin polarized and unpolarized states. We will study the effective theory of this system when when two gapping mechanisms are introduced: superconducting pairing and backscattering across interface, and show that it can support parafermions. Finally, we will exactly diagonalize the Hamiltonian with these two gapping terms within a suitably truncated Hilbert space. The resulting spectrum has six nearly degenerate states in some parameter regions, indicating the emergence of parafermion zero modes. Our results not only provide a new platform for realizing universal topological quantum computation, but also provide a general method to study the edge states between systems with different topological orders.

## 4.2 Analytic analysis of edge states on the boundary between $\frac{2}{3}$ spin polarized and unpolarized states

In this section, we will use the effective theory to analytically analyze the edge states structure for the boundary between $\frac{2}{3}$ spin polarized and unpolarized states, and quantitatively show that there are only two edge modes which propagate in different directions and have different spin polarizations. An analytic theory is essential here since it not only shed light on the numerical calculations in the following sections, but also is necessary for the study of the emergence of parafermions.

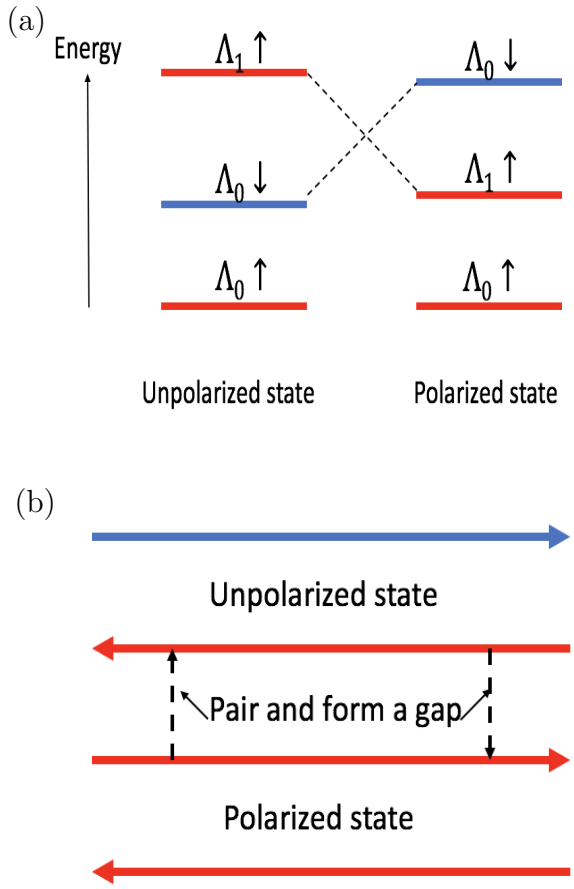


Figure 4.2. a: The schematic plot of the composite fermion energy levels in the bulk of the spin polarized and unpolarized regions. b: The possible edge modes on the boundary of spin polarized and unpolarized regions. The two modes in the middle corresponding to $\Lambda_{0\uparrow}$ can pair and form a gap, thus are removed from the low energy theory.

Before going into the quantitative theory, we first heuristically explain why there are edge states on the boundary between these two regions. The formation of edge modes are always related to the confinement potentials acting on the edges. However, naively it seems that there is no confinement potential around the internal edge in our case. Clever readers may realize that this simple observation is not true. We actually have intrinsic confinement potential in our case. From the analysis of last section, we see that there is a level crossing between the spin polarized and unpolarized states. The electrons in the $\Lambda_{0\downarrow}$ level of the spin unpolarized state can not tunnel into the spin polarized state since $\Lambda_{0\downarrow}$ level has a higher energy there. The same thing also happens for the electrons in $\Lambda_{1\uparrow}$ of spin polarized state, see Fig. 4.2(a). Therefore, the electrons in these two levels feel effective confinements and they form two edge modes. This situation is somewhat analogous to the Andreev bound states in the superconductor-normal-superconductor junction where single electron tunneling is forbidden below the superconducting gap. It is these intrinsic confinements that cause the formation of edge states. For the bottom level $\Lambda_{0\uparrow}$ on both sides, they may merge and there is no gapless excitations, see Fig. 4.2(b).

To quantitatively analyze the edge states, we apply the effective field theory methods reviewed in the last chapter. I rewrite the main results of the theory here. The Lagrangian density of the bulk effective theory for the fractional quantum Hall state can be written in the form [75, 76]:

$$\begin{aligned} \mathcal{L} &= -\frac{1}{4\pi} K_{II'} a_{I\mu} \partial_\nu a_{I'\lambda} \epsilon^{\mu\nu\lambda} - \frac{e}{2\pi} q_I A_\mu \partial_\nu a_{I\lambda} \epsilon^{\mu\nu\lambda} \\ &+ s_I \omega_\mu \partial_\nu a_{I\lambda} \epsilon^{\mu\nu\lambda} \end{aligned} \tag{4.2}$$

where $a_{I\mu}$ represent n Abelian Chern Simons (CS) gauge fields, $A_\mu$ is the electromagnetic gauge field, $\omega_\mu$ describes the curvature of the space, $\mathbf{K}$ is an n by n non-singular integer matrix describing the coupling between the CS gauge fields, $\mathbf{q}$ is an n-component integer vector describing the coupling between the CS gauge fields and the electromagnetic gauge field, $\mathbf{s}$ is an n-component half integer vector describing the coupling between the CS gauge fields and the curvature. An Abelian quantum

Hall state can be classified by a set $\{\mathbf{K}, \mathbf{q}, \mathbf{s}\}$ which determines the long distance properties of the state. Therefore, this set characterizes the topological order of the Abelian quantum Hall fluid [75, 76]. For our $\frac{2}{3}$ case, it takes the following value for the spin polarized case [76]:

$$\mathbf{K}_1 = \begin{pmatrix} 1 & 2 \\ 2 & 1 \end{pmatrix}, \mathbf{q}_1 = \begin{pmatrix} 1 \\ 1 \end{pmatrix}, \mathbf{s}_1 = \begin{pmatrix} \frac{1}{2} \\ -\frac{1}{2} \end{pmatrix} \tag{4.3}$$

for the spin unpolarized case:

$$\mathbf{K}_2 = \begin{pmatrix} 1 & 2 \\ 2 & 1 \end{pmatrix}, \mathbf{q}_2 = \begin{pmatrix} 1 \\ 1 \end{pmatrix}, \mathbf{s}_2 = \begin{pmatrix} \frac{1}{2} \\ \frac{1}{2} \end{pmatrix} \tag{4.4}$$

The form of the $\mathbf{K}$ matrix can be understood in terms of the CF picture [81]. For the $\frac{2}{3}$ state, there are two components each occupies a single CF Landau level in a effective antiparallel magnetic field, thus the $\mathbf{K}$ matrix is $K_{ij} = -\delta_{ij}$. Each component should be attached two flux, so we have to add 2 to each element of $\mathbf{K}$ matrix. The $\mathbf{q}$ represents the charge carried by each components of condensates. In the CF picture of $\frac{2}{3}$ states, all condensates should carry the same charge. The vector $\mathbf{s}$ is related to the Landau level occupied by each condensate. For spin unpolarized case, they both occupy the lowest Landau(or $\Lambda$) level thus have the same s. For spin polarized case, they occupy different Landau(or $\Lambda$) level thus have the different s. From Eqs. (4.3) and (4.4), we see that the only difference of spin polarized and unpolarized state is the spin vector $\mathbf{s}$. In Eq. (4.2) the second term and the third term are similar. So if we regard $\mathbf{q}$ as describing the unit of the electric charge carried by the two CF components, $\mathbf{s}$ can be regarded as describing the "curvature charge" carried by the CF components. Although the spaces in our problem are flat (disk and torus), the curvature charge still plays an important role in the properties of edge states as we will see later.

Now let's consider the edge physics. When the FQH liquid has boundaries, the action $S = \int dxdydt\mathcal{L}$, where $\mathcal{L}$ is given by Eq. (4.2), is not gauge invariant for the

CS gauge fields. To restore the gauge invariance, assuming the edge is along x axis, one has to introduce an action that describes the edge physics [76]:

$$\mathcal{S}_{edge} = \frac{1}{4\pi}\int dtdx[\mathbf{K}_{IJ}\partial_t\phi_I\partial_x\phi_J - \mathbf{V}_{IJ}\partial_x\phi_I\partial_x\phi_J] \tag{4.5}$$

In the above equation, $\phi_I$ is the field that describes the $I$th component of the edge branches, $a_{Ii} = \partial_i\phi_I$ and $\rho_I = \frac{1}{2\pi}\partial_x\phi_I$ is the density of the ith branch. $\mathbf{K}$ is the same matrix as the bulk state, and one can show that its positive eigenvalues correspond to left-moving branches and negative to right-moving branches. $\mathbf{V}$ is a positive-definite matrix that encodes the non-universal interactions between edge branches. Now we want to study the properties of the edge between two Abelian FQH states. Assuming the edge is along $y = 0$ axis, using the same gauge argument as in Ref. [76], we find out the $\{\mathbf{K}, \mathbf{q}, \mathbf{s}\}$ for the new state is

$$\mathbf{K} = \mathbf{K}_1 \bigoplus -\mathbf{K}_2, \mathbf{q} = \mathbf{q}_1 \bigoplus \mathbf{q}_2, \mathbf{s} = \mathbf{s}_1 \bigoplus \mathbf{s}_2 \tag{4.6}$$

A similar situation has been considered in Ref. [94], but they omit the role of spin vectors. Now we improve their method by putting spin vectors into consideration. In Eq. (4.6), $dim(K) = dim(K_1) + dim(K_2)$ and all edge branches are retained. After considering the tunneling perturbation, we will see some of the edge branches may be removed from the low energy theory. Now, according to Ref. [94], we define the following quantities:

$$\begin{aligned} \phi(m) = m_i\phi_i, \quad q(m) = m_iq_i, \\ s(m) = m_is_i, \quad K(m) = m_iK_{ij}m_j \end{aligned} \tag{4.7}$$

where $\mathbf{m}$ is an integer valued vector and repeated indexes means summation. We define a set of local fields [94]:

$$\Psi_m = e^{-i\phi(m)} \tag{4.8}$$

which obey, for $x \neq x'$,

$$\Psi_m(x)\Psi_{m'}(x') = (-1)^{q(m)q(m')}\Psi_{m'}(x')\Psi_m(x) \tag{4.9}$$

In the symmetric representation, from the properties of **K** matrix, we have:

$$(-1)^{K(m)} = (-1)^{q(m)} \tag{4.10}$$

Thus, if $K(m)$ is odd, the field $\Psi_m$ is fermionic, and if $K(m)$ is even, it is bosonic. Now we consider the tunneling perturbation [94]:

$$T = \int dx[t(x)\Psi_m(x) + h.c.] \tag{4.11}$$

It should be bosonic and charge conserving so $q(m) = s(m) = 0$ and $K(m)$ even. In Ref. [94], they only require $q(m) = 0$ and $K(m)$ even. We argue that **s** also represents the internal structure of the fractional quantum Hall liquid. From the similarity of **q** and **s** terms in Eq. (4.2), we also require $s(m) = 0$. The scaling dimension of $\Psi_m$ is $\Delta(m)$ that satisfies the inequality [94]:

$$\Delta(m) \geqslant \frac{1}{2}|K(m)| \tag{4.12}$$

If the tunneling perturbation is relevant, the modes in $\Psi_m$ become massive and are removed from the low energy theory. From the scaling perspective it is potentially relevant if the scaling dimension $\Delta(m) < 2$. So, with the constraints given above, we conclude that the condition for **m** that leads to a potentially mass generating perturbation is that [94]:

$$K(m) = q(m) = s(m) = 0 \tag{4.13}$$

Although the space may be flat, the spin vector still plays a role in the properties of edge states.

We now apply this analysis to the edge states between $\frac{2}{3}$ spin polarized and unpolarized states. The $\{\mathbf{K}, \mathbf{q}, \mathbf{s}\}$ of the effective theory for this phase coexistence state is:

$$\mathbf{K} = \begin{pmatrix} 1 & 2 & 0 & 0 \\ 2 & 1 & 0 & 0 \\ 0 & 0 & -1 & -2 \\ 0 & 0 & -2 & -1 \end{pmatrix}, \mathbf{q} = \begin{pmatrix} 1 \\ 1 \\ 1 \\ 1 \end{pmatrix}, \mathbf{s} = \begin{pmatrix} \frac{1}{2} \\ \frac{1}{2} \\ \frac{1}{2} \\ -\frac{1}{2} \end{pmatrix} \tag{4.14}$$

In terms of CF theory, we can identify fields $\phi_i$ as $\phi_1$, $\phi_2$ corresponding to $\Lambda_{0\uparrow}$, $\Lambda_{0\downarrow}$ respectively, and $\phi_3$, $\phi_4$ corresponding to $\Lambda_{0\uparrow}$, $\Lambda_{1\uparrow}$ respectively. From Eqs. (4.13) and (4.14), we find out two independent solutions for $\mathbf{m}$: $\mathbf{m}_1 = (1, 0, -1, 0)$ and $\mathbf{m}_2 = (0, 1, -1, 0)$. $\mathbf{m}_2$ represents tunneling between $\Lambda_{0\downarrow}$ and $\Lambda_{0\uparrow}$ which is unlikely to happen since there is an energy gap. Therefore, only the operator $\Psi_{m_1}$ is relevant and potentially mass generating, and $\phi_1$, $\phi_3$ are removed from the low energy theory. So we conclude that there are only two counter-propagating edge states represented by $\phi_2$ and $\phi_4$ remaining in the low energy regime and they have different spin polarizations.

## 4.3 Numerical calculations on the disk

In this section, we will use the numerical method to confirm the conclusions in the last section about the induced edge states between $\frac{2}{3}$ spin polarized and unpolarized states. Some of the results are discussed in our paper Ref. [96].

We simulate a system of 8 electrons in a magnetic field using the disk geometry shown schematically in Fig. 4.3(a). In this model we use a spatially dependent Zeeman energy to control spin polarization of the 2DEG, see Fig. 4.3(b). The central region of the disk of radius $R_1$ is characterized by a large Zeeman term $E_Z^{max}$, while the outer region with outer diameter $R_2$ is set to $E_Z^{min} = 0$. The Zeeman term is varied smoothly within the region $R_1 < r < R_1 + \Delta R$, resulting in a smooth variation of wavefunctions across the disk and avoiding spurious effects originating from abrupt changes. When there are 8 electrons on the disk, the allowing single particle states have angular momentum $0 \leqslant m \leqslant 11$. Thus, $R_2 = \sqrt{22} l_m = 4.8 l_m$. We want the central region contains half of the electrons so $R_1 + \Delta R = \sqrt{11} l_m = 3.3 l_m$. We set $R_1 = 2.9 l_m$ and $\Delta R = 0.4 l_m$. We anticipate the electrons spin polarized in the central region and unpolarized in the outer region. Note that due to a strong penetration of electron wavefunction from the outer $R_1 < r < R_2$ region into the inner $r < R_1$ region the difference of the average spin splitting $\int \psi(r)^* E_Z(r) \psi(r) d^2 r$ for the modes on the two sides of the domain wall is $< 6\%$, similar to the experimental conditions.

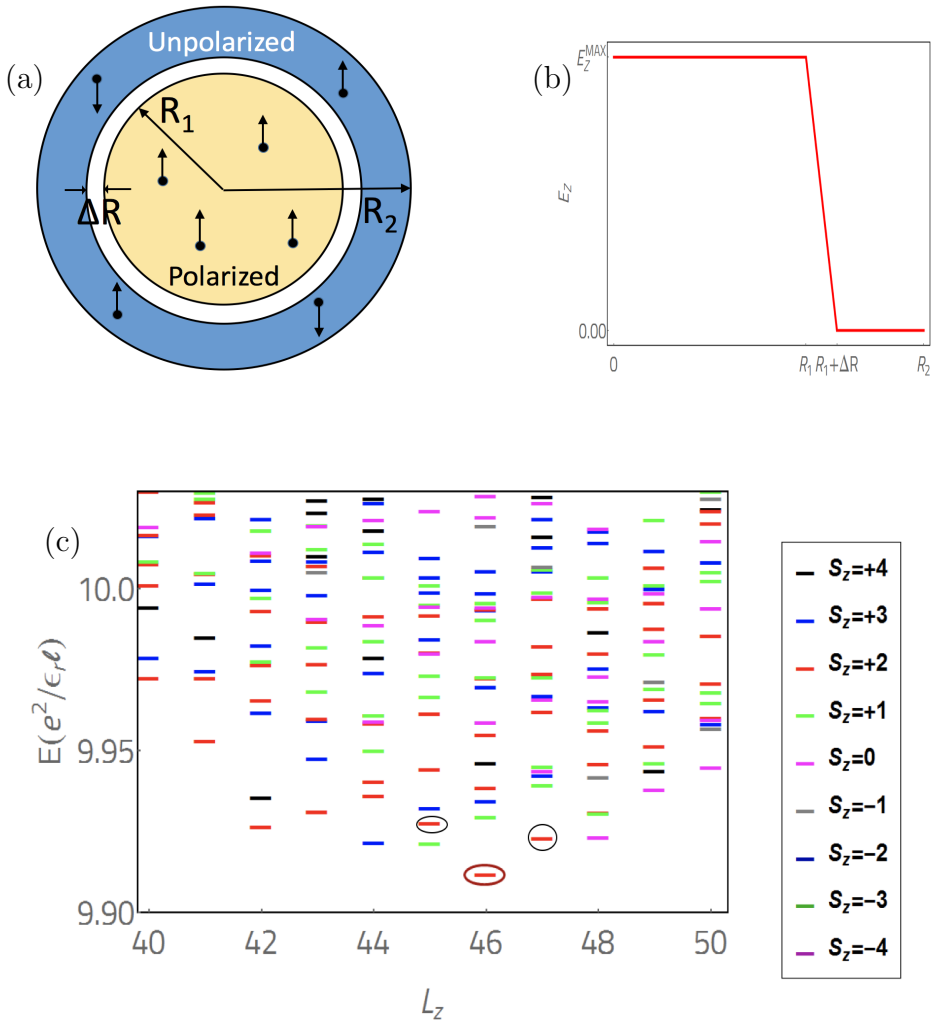


Figure 4.3. a: Disk geometry for the simulation domain. b: Profile of Zeeman energy. c: Spectra of 8 electrons on the disk with profile of Zeeman energy show in Fig. 4.3(b). They are characterized by total angular momentum $L_z$ and total spin $S_z$ of particles. Edge excitations with the same $S_z = 2$ as in the ground state and with $L_z = 45, 47$, which correspond to the addition or subtraction of a single flux, are circled black.

The Hamiltonian is given by:

$$\begin{aligned}\mathcal{H}_d &= \frac{1}{2m^*}\sum_i(\mathbf{p}+\frac{e\mathbf{A}}{c})_i^2 + E_z(r_i)\sigma_z^{(i)} + U_i \\ &+ \sum_{ij}\frac{e^2}{\epsilon|r_i-r_j|}\end{aligned} \tag{4.15}$$

The first term and the second term are kinetic energy and Zeeman energy respectively. The third term is the parabolic confinement $U(r) = Cr^2$ with $C = 0.036e^2/\epsilon l_m^3$ and the last term is the Coulomb interaction. This Hamiltonian is diagonalized using a configuration interaction method. The states are classified by their projections of total angular momentum on z-axis, $L_z$ and the total spin of electrons, $S_z$. We exactly diagonalize this Hamiltonian for 8 electrons in a varying Zeeman energy that models the coexistence of spin polarized and unpolarized states at a filling factor 2/3. The spectra are given in Fig. 4.3(c). We identified the ground state, which is spin-polarized in the center and unpolarized in the outer region of the disk, as well as the edge states flowing close to the boundary between spin polarized and spin unpolarized regions. Their number and spin density distributions are calculated. All of the results are shown in Fig. 4.4(a)-4.4(f).

The ground state has total angular momentum $L_z = 46$ and total spin $S_z = 2$. The total spin indicates that 6 electrons are in spin up states and 2 electrons are in spin down states, as expected. In the CF picture, there are N electrons with N/2 occupying $\Lambda_{0\uparrow}$ and N/4 occupying $\Lambda_{1\uparrow}$ in the center region and $\Lambda_{0\downarrow}$ in the outer region. The total angular momentum of the ground state is (Note that for Landau level n, the angular momentum index start from -n in the symmetric gauge):

$$\begin{aligned}L_z &= pN(N-1) + L_z^{CF} = N(N-1) \\ &- (\frac{N}{4}(\frac{N}{2}-1) + (\frac{N}{4}-3)\frac{N}{8} + (\frac{3N}{4}-1)\frac{N}{8} \\ &= N(N-1) - \frac{N(N-3)}{4} = \frac{N(3N-1)}{4}\end{aligned} \tag{4.16}$$

For N=8, $L_z = 46$ indeed, coinciding with the numerical result. The ground state is separated by a gap from the rest of the spectra, see Fig. 4.3(c) and does not carry

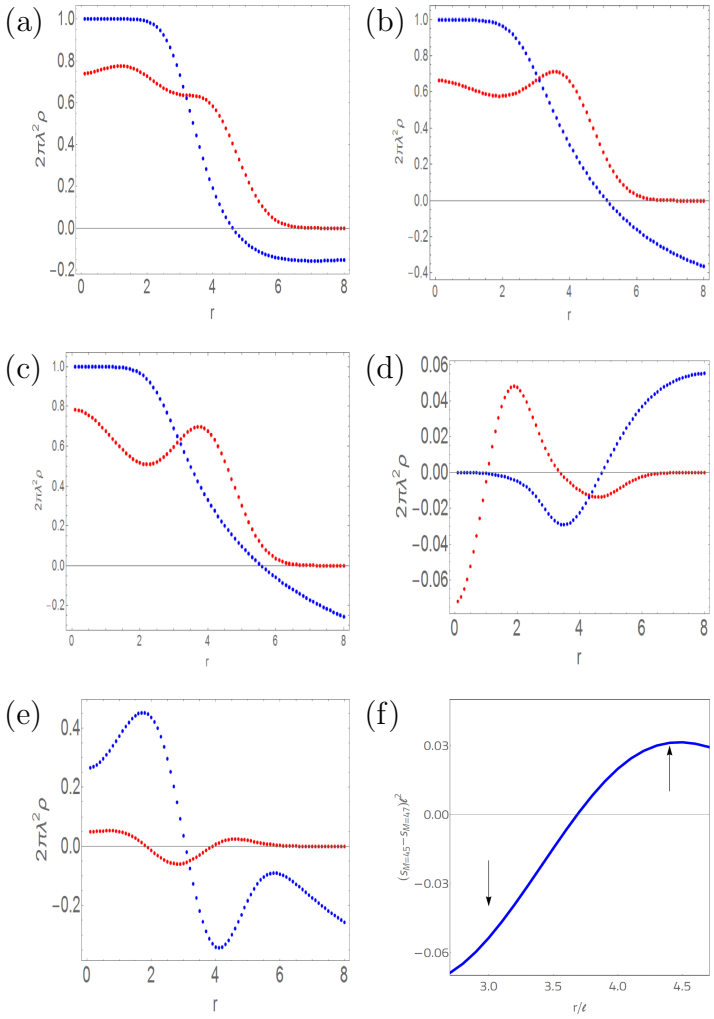


Figure 4.4. a: The ground state electron density (red) and spin density (blue) for 8 electrons on a disk containing the domain wall between polarized and unpolarized states at a filling factor 2/3 in a magnetic field. b: The density profile (red) and spin polarization (blue) for the edge state $M = 45$. c: The density profile (red) and spin polarization (blue) for the edge state $M = 47$. d: The differences of density (red) and spin (blue) between $M = 45$ edge state and the ground state. e: The differences of density (red) and spin (blue) between $M = 47$ edge state and the ground state. f: Spin difference between edge state $M = 45$ and $M = 47$.

current. From the spin profile in Fig. 4.4(a), the ground state is indeed spin polarized in the center of the disk and unpolarized in the outer region of the disk.

The lowest energy excitations which have spin polarization of the ground state and correspond to a single flux addition or subtraction have $L_z = 45$ and $L_z = 47$, see Fig. 4.4(b) and Fig. 4.4(c). These are the modes that carry electrical current. when compared to the ground state, they have $\Delta L = -1$ and $\Delta L = 1$ respectively. This indicates that these two edge states have opposite linear velocities. The differences of density and spin polarization between the two edge states and the ground state are shown in Fig. 4.4(d) and Fig. 4.4(e). We observe that the density differences have large value only around the internal edge, which confirms that the two edge states correspond to the internal edge. In Fig. 4.4(f), we show the results for the difference of spin densities of the two modes near the domain wall between polarized and unpolarized region. Despite the finite size effects in a small system, the exact diagonalization clearly identify that the two edge states in the domain wall region have components of spin density with opposite orientation. Our numerical study clearly show that there are two counter-propagating edge states in the domain wall with different spin polarizations, which is consistent with our analysis in the previous section.

## 4.4 Numerical calculations on the torus

In this section, we will numerically study the system in a torus geometry. The advantage of the torus geometry is that it gets rid of the edge between the FQH liquid and the vacuum, so the physics related to the induced edge between spin polarized and unpolarized states become clear.

The torus geometry is basically a rectangular cell with periodic boundary conditions. This geometry has been considered in Ref. [97] for $\frac{1}{3}$ FQH state. We apply their method to our case. We take the coordinate system such that the boundary of the rectangular cell is given by $x = 0, x = a, y = 0, y = a$, with vector potential $\vec{\mathbf{A}} = (0, xB)$.

We have $2\pi l_B^2 \frac{N}{a^2} = \nu$, so $a = \sqrt{24\pi} l_B = 8.68 l_B$, and there are $m = \frac{N}{\nu} = 12$ single electron orbitals in the cell.

The wave functions of these orbitals are [97]:

$$\phi_j(\vec{r}) = (\frac{1}{a\pi^{1/2} l_B})^{\frac{1}{2}} \sum_{k=-\infty}^{\infty} e^{[i\frac{(X_j+ka)y}{l_B^2} - \frac{(X_j+ka-x)^2}{2l_B^2}]} \tag{4.17}$$

where $j$ labels the jth orbit, $1 \leqslant j \leqslant m$, and $X_j = \frac{j}{m}a$ is the center coordinate of the cyclotron motion. The Hamiltonian of the system can be written as:

$$\begin{aligned} \mathcal{H}_t &= \frac{1}{2m^*} \sum_i (\mathbf{p} + \frac{e\mathbf{A}}{c})_i^2 + E_z(r_i)\sigma_z^{(i)} \\ &+ \sum_{ij} V(\mathbf{r}_i - \mathbf{r}_j) \end{aligned} \tag{4.18}$$

The first and second terms are kinetic and Zeeman terms respectively. The third term is the Coulomb interaction and due to the boundary condition, it is given by [97]:

$$V(\mathbf{r}) = \sum_s \sum_t \frac{e^2}{\epsilon|\mathbf{r} + sa\hat{x} + ta\hat{y}|} \tag{4.19}$$

Its matrix elements are the following [97]:

$$\begin{aligned} V_{j_1 j_2 j_3 j_4} &= \frac{1}{2} \int d^2 r_1 d^2 r_2 \phi_{j_1}^*(\mathbf{r}_1) \phi_{j_2}^*(\mathbf{r}_2) V(\mathbf{r}_1 - \mathbf{r}_2) \phi_{j_3}(\mathbf{r}_3) \phi_{j_4}(\mathbf{r}_4) \\ &= \frac{1}{2a^2} \sum_q{}' \sum_s \sum_t \delta_{q_x, \frac{2\pi s}{a}} \delta_{q_y, \frac{2\pi t}{a}} \delta'_{j_1 - j_4, t} \frac{2\pi e^2}{\epsilon q} \\ &\times exp[-\frac{l_B^2 q^2}{2} - 2\pi i s \frac{j_1 - j_3}{m}] \delta'_{j_1 + j_2, j_3 + j_4} \end{aligned} \tag{4.20}$$

The symbols with prime mean that they are defined modulo $m$ and the summation over $q$ excludes $q = 0$. From the above expression we observe that the total momentum is conserved only modulo $m$. Therefore, we use the total momentum (mod m) $M$ and the total spin $S$ to classify the states.

We first exact diagonalize the Hamiltonian for 8 electrons in the lowest Landau level when there are no Zeeman term. In this case, only the Coulomb term plays a role. The spectra of the Hamiltonian are given in Fig. 4.5(c). We find that the ground state degeneracy is 3, which is consistent with Ref. [98] where the degeneracy is given by $|det(K)|$ and Eq. (4.4) indeed gives 3.

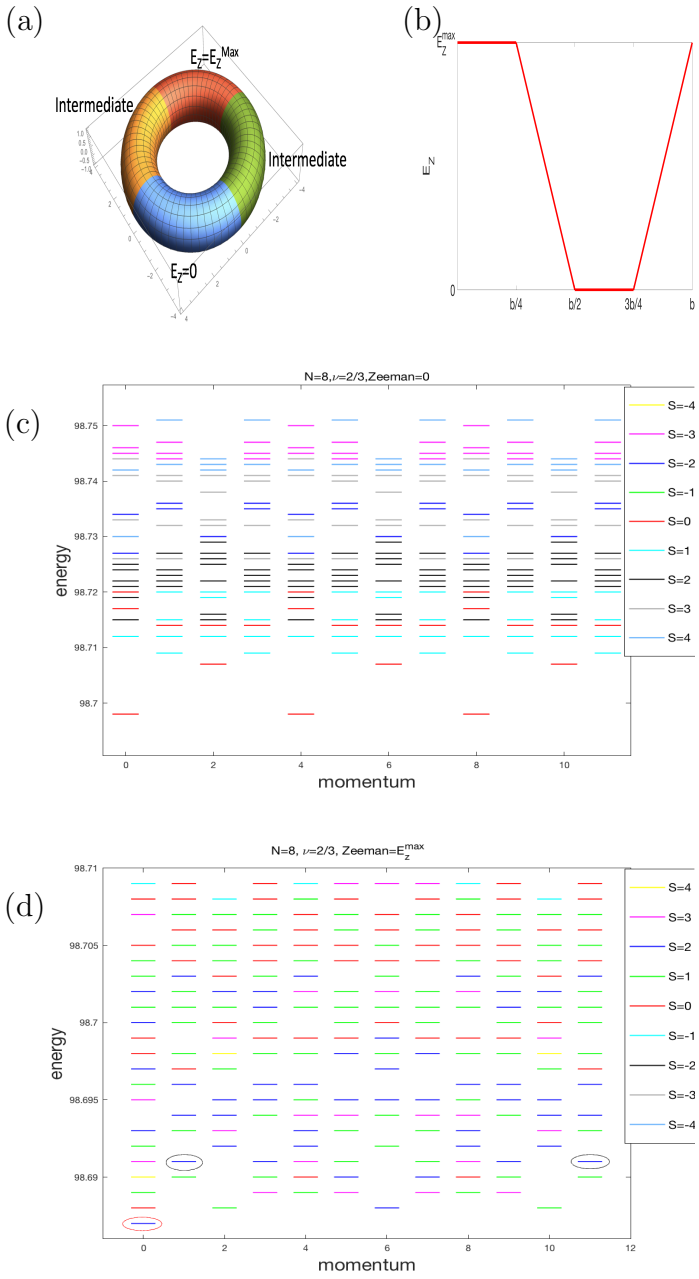


Figure 4.5. a: The torus geometry for a varying Zeeman energy. b: The amplitude of Zeeman energy along the toroidal direction. c: Spectra of 8 electrons on the torus without Zeeman splitting. The ground state has 3 fold degeneracy. d: Spectra of 8 electrons on the torus with profile of Zeeman energy show in Fig. 4.5(b). They are characterized by total momentum (mod 12) $L_z$ and total spin $S_z$ of particles. Ground state is in $L_z = 0$ and $S_z = 2$, circled red. Edge excitations with the same $S_z = 2$ as in the ground state with $L_z = 1, 11$, which correspond to the addition or subtraction of a single flux, are circled black.

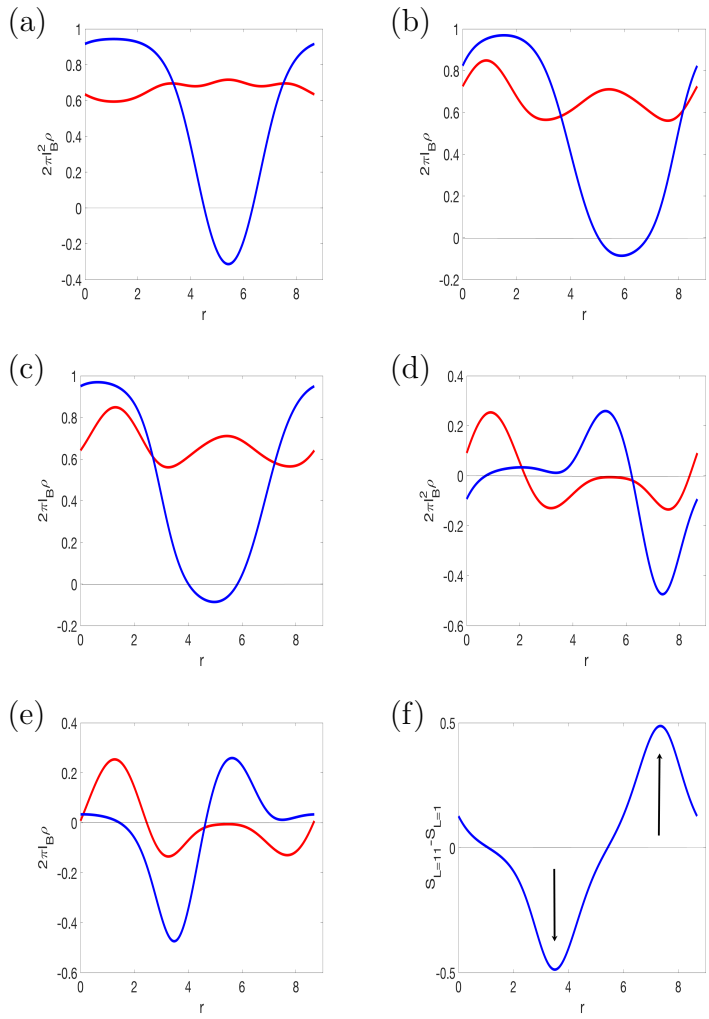


Figure 4.6. a: The ground state electron density (red) and spin density (blue) for 8 electrons on a torus containing the domain wall between polarized and unpolarized states at a filling factor 2/3 in a magnetic field. b: The density profile (red) and spin polarization (blue) for the edge state $M = 1$. c: The density profile (red) and spin polarization (blue) for the edge state $M = 11$. d: The differences of density (red) and spin (blue) between $M = 1$ edge state and the ground state. e: The differences of density (red) and spin (blue) between $M = 11$ edge state and the ground state. f: Spin difference between edge state $M = 11$ and $M = 1$.

Now we turn on the Zeeman term and let it has space dependent as Fig. 4.5(a) and 4.5(b). The torus are divided into four equal regions. One of them has large Zeeman energy $E_Z^{max}$ and its opposite side has zero Zeeman energy. The regions between them vary smoothly form zero to $E_Z^{max}$. Exact diagonalization of the Hamiltonian gives a spectra Fig. 4.5(d). We see that there is a single ground state with $M = 0$ and $S = 2$ circled red in Fig. 4.5(d). The reason for the lift of the degeneracy is due to the broken of the magnetic translation symmetry when a spatially varying Zeeman term is included in the Hamiltonian.

We find out the density profile and the spin polarization of the ground state, see Fig. 4.6(a). Its density is fluctuating slightly around $\nu = 2/3$ as expected. The spin polarization is almost 1 within the region where $E_Z = E_Z^{max}$ (region A) and has a dip in the region $E_Z = 0$ (region B). This clearly indicates that the electrons are spin polarized in region A and spin unpolarized in region B. Therefore, our numerical calculation indeed simulate the phase coexistent state.

Now, let's look at the edge states. Comparing Fig. 4.5(c) and Fig. 4.5(d), it should be clear that there are lots of low energy excitations. We are most interested in the two states with the same total spin as the ground state and correspond to single edge state quanta flowing in the positive and negative poloidal directions. They are circled black in Fig. 4.5(d) with total spin 2 their momentum are $L = 1$ and $L = 11$ respectively. Their density distributions and spin polarizations, as well as the differences between them and the ground state are calculated, see Fig. 4.6(b) - Fig. 4.6(e). In order to compare the spin polarizations of the edge states, we also calculate $S_{11} - S_1$ and plot it in Fig. 4.6(f). It indeed shows a spin transition around one edge between region A and B. Therefore, our numerical study on the torus also support the conclusion that there are two counter-propagating edge states with different spin polarizations in the domain wall between spin polarized and spin unpolarized states.

## 4.5 Emergence of parafermion modes

From the analytic analysis and numerical calculations, we are convinced that the edge states have opposite components of velocity and spin. Therefore, these states can potentially be coupled to an s-wave superconductor, a pre-requisite for generating topological superconductivity. In integer quantum Hall ferromagnets, proximity superconducting coupling has resulted in topological superconductivity in the domain wall region and Majorana zero modes at the boundaries between topological trivial and non-trivial superconducting regions [90]. In the FQH regime, we anticipate the appearances of parafermions due to the fractional charges and fractional statistics. in this section, we will quantitatively show how the parafermions emerge when coupled to an s-wave superconductor and a spin orbit coupled insulator.

The physics of the edge modes are given by the action Eq. (4.5) with $K$ matrix given by Eq. (4.14). To simplify the expressions, we redefine the fields $\phi_{11} = \phi_1$, $\phi_{12} = \phi_2$, $\phi_{21} = \phi_3$, $\phi_{22} = \phi_4$. After quantizing these fields, we have the following commutation relations [13, 66]:

$$[\phi_{1\alpha}(x), \phi_{1\beta}(x')] = i\pi[(K^{-1})_{\alpha\beta}\mathrm{sgn}(x-x') + i\sigma^y_{\alpha\beta}] \tag{4.21}$$

$$[\phi_{2\alpha}(x), \phi_{2\beta}(x')] = i\pi[(-K^{-1})_{\alpha\beta}\mathrm{sgn}(x-x') + i\sigma^y_{\alpha\beta}] \tag{4.22}$$

$$[\phi_{1\alpha}(x), \phi_{2\beta}(x')] = i\pi[(-K^{-1})_{\alpha\beta} + i\sigma^y_{\alpha\beta}] \tag{4.23}$$

From the analysis of Sec.II, the remaining edge modes are generated by the fields $\phi_2$ and $\phi_4$. From Eq. (4.21) to (4.23), we find their commutation relation are:

$$[\phi_2(x), \phi_2(x')] = \frac{i\pi}{3}\mathrm{sgn}(x-x') \tag{4.24}$$

$$[\phi_4(x), \phi_4(x')] = -\frac{i\pi}{3}\mathrm{sgn}(x-x') \tag{4.25}$$

$$[\phi_4(x), \phi_2(x')] = \frac{i\pi}{3} \tag{4.26}$$

Therefore, $\phi_2$ and $\phi_4$ satisfy exactly the same commutation relations as $\phi_R$ and $\phi_L$ in Ref. [64]. We can follow their method to show the emergence of parafermions.

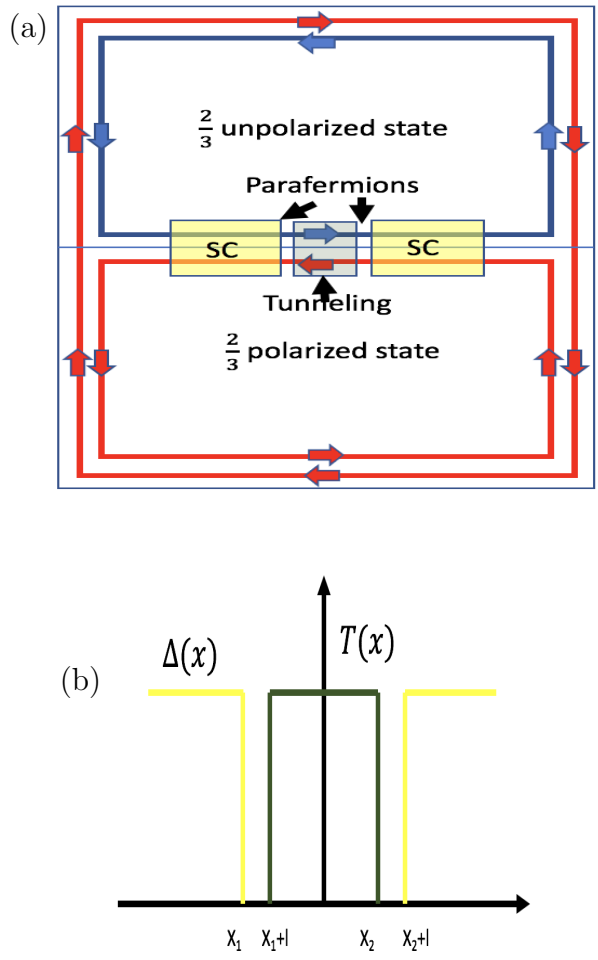


Figure 4.7. a: A schematic plot of experimental realization of parafermion zero modes. b: The spatial profile of the superconducting pairing and backscattering tunneling amplitudes $\Delta(x)$ and $T(x)$ induced by proximity effects in Fig.4.7(a) [64].

We consider the architecture in Fig.4.7(a). The two counter-propagating, opposite spin edge states are put in close proximity to alternating s-wave superconducting and backscattering tunneling regions. The amplitudes of the pairing potential and tunneling are given in Fig. 4.7(b). Redefine the fields $\phi_{2/4} = \varphi \pm \theta$. The Hamiltonian of the interface are given by $H = H_0 + H_1$, where [64]

$$H_0 = \frac{mv}{2\pi} \int dx[(\partial_x \varphi)^2 + (\partial_x \theta)^2] \tag{4.27}$$

$m = 3$ and [64]

$$H_1 \sim \int dx[-\Delta(x)cos(2m\varphi) - T(x)cos(2m\theta)] \tag{4.28}$$

One can write $\varphi_{x<x_1} = \pi n_\varphi^1/m$, $\theta_{x\epsilon(x_1+l,x_2)} = \pi n_\theta/m$, $\varphi_{x>x_2+l} = \pi n_\varphi^2/m$, and we have [64]:

$$[n_\varphi^2, n_\theta] = i\frac{m}{\pi} \tag{4.29}$$

At low energy, we can focus on the interval regions between $x_j$ and $x_j + l$. They are governed by the effective Hamiltonian [64]

$$H_{eff} = \frac{mv}{2\pi} \sum_{i=1}^{2} \int_{x_i}^{x_i+l} dx[(\partial_x \varphi)^2 + (\partial_x \theta)^2] \tag{4.30}$$

We can thus identify the operators [64]

$$a_j \to e^{i(\pi/m)(n_\varphi^j + n_\theta)} \tag{4.31}$$

which commute with $H_{eff}$ and thus represent zero modes bound to the domain walls. They have relations:

$$a_j^{2m} = 1, a_j a_{j'} = a_{j'} a_j e^{i(\pi/m)sgn(j'-j)} \tag{4.32}$$

Therefore, they are parafermion operators and they produce a 2m fold ground state degeneracy.

## 4.6 Numerical Calculations for Parafermionic Zero Modes

Based on the results in the last section, we now show that the parafermions can emerge if the s-wave superconductivity and tunneling are properly introduced into

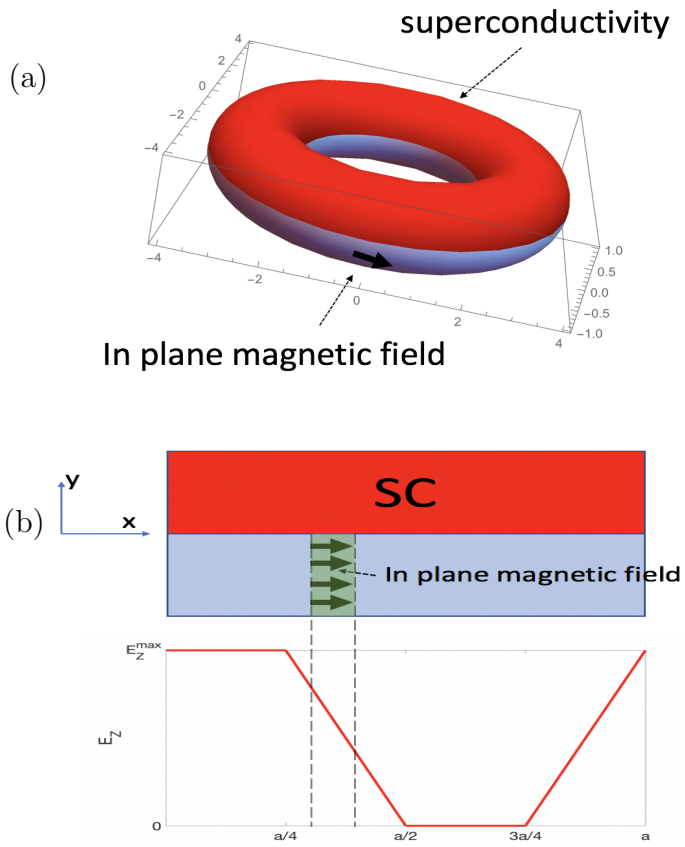


Figure 4.8. a: A schematic plot of our system. The superconductivity is introduced only on the top half of the torus. An in-plane magnetic field is introduced on the bottom half of the torus but is confined in the domain wall region. b: (top)The rectangular representation of the torus. The green shaded region has an in-plane magnetic field and it's located near one of the domain walls. (bottom)The profile of the Zeeman coupling in the z direction which is perpendicular to the surface of the rectangular. Domain walls form in two regions [a/4, a/2] and [3a/4, a].

the quantum Hall states. In our system, the appearance of parafermion modes is indicated by the appearance of six-fold nearly degenerate ground states.

The Hamiltonian of the system can be written as:

$$\mathcal{H} = \mathcal{H}_t + H_{SC} + H_{BX} - \mu\hat{N} + C(\hat{N} - \hat{N}_0)^2 \tag{4.33}$$

The first term $\mathcal{H}_t$ is given by Eq. (4.18). As illustrated in previous sections, two domain walls form in the boundary regions between the spin polarized and unpolarized states. The boundary regions are the intermediate regions between $E_Z^{max}$ and 0 in Fig. 4.8(b), which are [a/4, a/2] and [3a/4, a]. Each domain wall support a pair of counter-propagating edge modes with different spin polarizations. The second term $H_{SC}$ is the superconducting pairing term

$$H_{SC} = \int d\mathbf{r}(\Delta(\mathbf{r})\Psi_\uparrow^\dagger(\mathbf{r})\Psi_\downarrow^\dagger(\mathbf{r}) + \Delta^*(\mathbf{r})\Psi_\downarrow(\mathbf{r})\Psi_\uparrow(\mathbf{r})) \tag{4.34}$$

where the $\Delta(\mathbf{r})$ takes constant value $\Delta_1$ on the top half of the torus and $\Delta_2$ on the bottom half of the torus. In our simulations, $\Delta_2 = 0$, see Fig. 4.8(a). If we express the field operators $\Psi(\mathbf{r})$ in terms of the creation and annihilation operators $a_j^\dagger$ and $a_j$ which add or annihilate an electron in states given by Eq. (4.17), we have $H_{SC} = \sum_{j,n} \Delta_{jn} a_{j\uparrow}^\dagger a_{n\downarrow}^\dagger + H.c.$, with $j, n = 1, 2, ..., m$. When the total number of states m is an even number, we have for $j + n = m, 2m$:

$$\begin{aligned} \Delta_{jn} &= \sum_{k+q=-1} \frac{\Delta_1 + \Delta_2}{2\sqrt{\pi}} \int_0^a dx \exp(-[\frac{(X_j + ka - x)^2}{2} \\ &+ \frac{(X_n + qa - x)^2}{2}]) \end{aligned} \tag{4.35}$$

where $X_j = a\frac{j}{m}$, and for $j + n$ =odd numbers:

$$\begin{aligned} \Delta_{jn} &= \sum_{k,q} \frac{i(\Delta_2 - \Delta_1)}{2\pi^{\frac{3}{2}} m(k + q + \frac{j+n}{m})} \int_0^a dx \exp \\ &( -[\frac{(X_j + ka - x)^2}{2} + \frac{(X_n + qa - x)^2}{2}]) \end{aligned} \tag{4.36}$$

The third term $H_{BX}$ is a spin flipping tunneling term. In this paper, we take it to be an in plane Zeeman coupling along the x axis (x and y directions of the torus are

defined in Fig.4.8(b)), but it may be generated by other methods. We have $H_{BX} = \sum_i \frac{1}{2} g\mu B(\mathbf{r_i})\sigma_x^{(i)}$. In our numerical calculations, $B(\mathbf{r}) = B$ if $x \in [0.35a, 0.45a]$ and $y \in [0, 0.5a]$, where $a$ is the length of the torus in x and y directions. Otherwise $B(\mathbf{r}) = 0$ as shown in Fig. 4.8(b). In second quantization form, $H_{BX} = \sum_{j,n} B_{jn} a^\dagger_{j\uparrow} a_{n\downarrow} + H.c.$, with $j, n = 1, 2, ..., m$. When $j = n$, we have:

$$\begin{aligned} B_{jn} &= \sum_{k=q} \frac{g\mu B}{4\sqrt{\pi}} \int_{0.35a}^{0.45a} dx \exp(-[\frac{(X_j + ka - x)^2}{2} \\ &+ \frac{(X_n + qa - x)^2}{2}]) \end{aligned} \tag{4.37}$$

when $j - n$ = odd numbers:

$$\begin{aligned} B_{jn} &= \sum_{k,q} i \frac{g\mu B}{2\pi^{\frac{3}{2}} m(k - q + \frac{j-n}{m})} \int_{0.35a}^{0.45a} dx \exp \\ &( -[\frac{(X_j + ka - x)^2}{2} + \frac{(X_n + qa - x)^2}{2}]) \end{aligned} \tag{4.38}$$

The fourth term is the chemical potential and the fifth term is the charging energy which is similar to that introduced in [99]. It can be regarded as the capacitor energy associated with the change of the number of electrons. These two terms are used to tune the electron number of the ground state of the system to the desired number. However, as we will see later, they are small in values when compared with $H_{SC}$ and $H_{BX}$ and we consider only a small number of particles, therefore these two terms do not affect our results. For large number of particles they may be relevant so we include them in the Hamiltonian.

Now let's discuss the Hilbert space of our numerical simulations. We put 4 electrons in the 6 orbitals defined in Eq.(4.17), so $m = 6$. Half of the electrons are in the spin polarized state and half in spin unpolarized state, thus 3 electrons are spin up, and 1 is spin down, total spin $S = 1$. We use (N, S) to represent the set of states with total electron number N and total spin S. Without superconductivity and tunneling, the space is (4, 1). The $H_{SC}$ mixes the states with different numbers and $H_{BX}$ mixes the states with different total spins, therefore our Hilbert space in numerical calculation is the set {(6, 2), (6, 1), (6, 0), (4, 2), (4, 1), (4, 0), (2, 1), (2, 0)}.

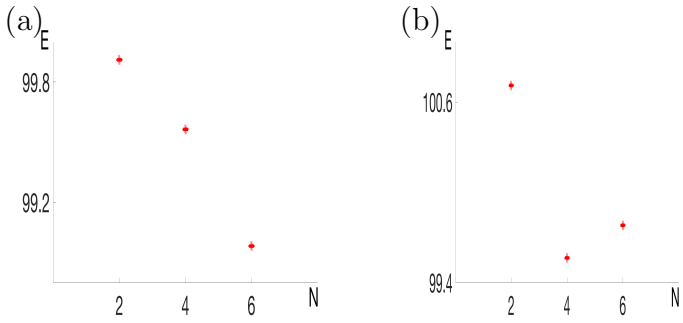


Figure 4.9. a: The lowest energies in $N = 2, 4, 6$ sectors of $\mathcal{H}_t$. b: Including $\mu = 0$, $C = 0.2$, the lowest energies has been shifted so $N = 4$ sector has the lowest energy and it's in the (4,1) sector.

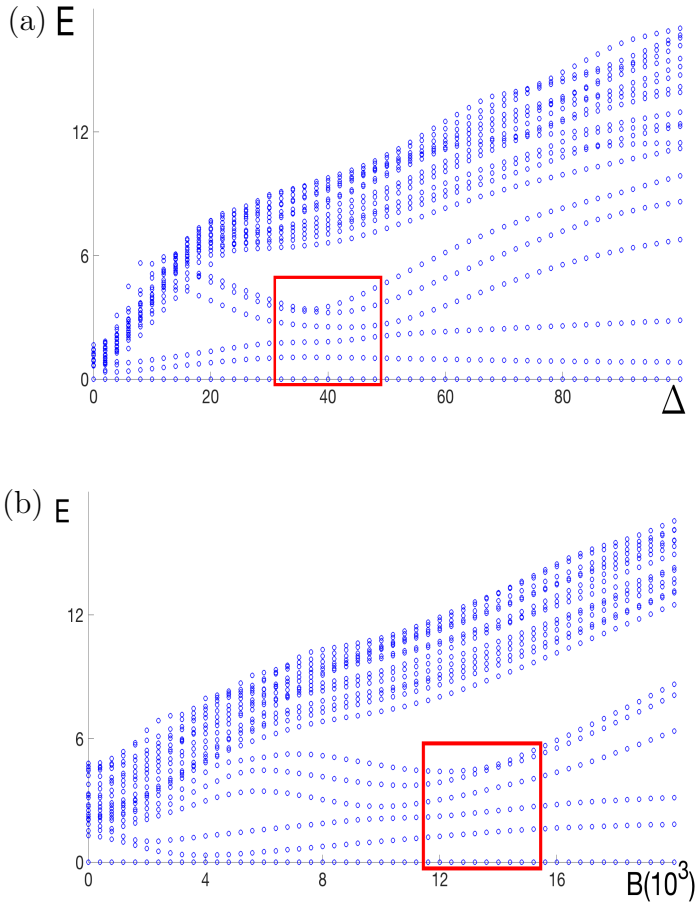


Figure 4.10. a: The energy spectrum versus superconducting pairing potential $\Delta$ with a fixed $B$ = 10000. The red rectangular indicates the six fold degenerate ground state sup-space which are separated from the bulk by a gap. This is the evidence for the appearance of parafermion modes. b: The energy spectrum versus in plane magnetic field with a fixed $\Delta$ = 50. The six fold ground state degeneracy also appears and it lasts for a broader parameter regime. The energy unit is given by $\frac{e^2}{\epsilon l_B}$. The unit for the field is Tesla.

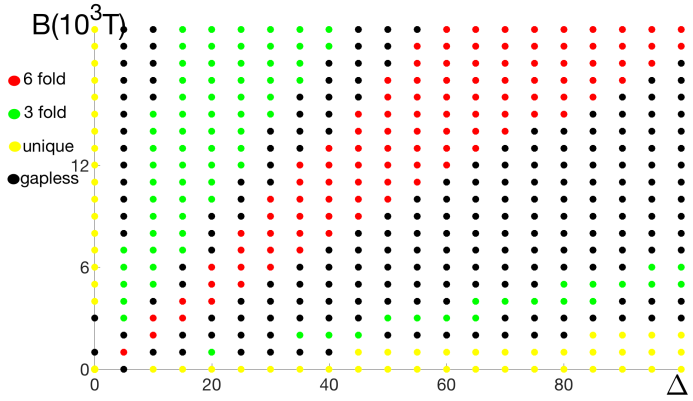


Figure 4.11. The phase diagram of our system. The red region represents states which has six fold ground state degeneracy. The green region represents states which has three fold ground state degeneracy and yellow region represents states with a unique ground state. Black region represents gapless states. To be qualified as a gap, the max energy difference between suspected states should be at least two times as large as the second max energy difference. In this phase diagram we observe that the six fold ground state degeneracy regime are separated from other gapped states by gapless regions, which means that a quantum phase transition may occur when we go from one regime to another regime. Therefore we can call the phase represented by the red region as the topological superconducting phase that supports parafermionic zero modes.

If the Hamiltonian contains only $\mathcal{H}_t$, the lowest energies of the $N = 2, 4, 6$ sectors are shown in Fig. 4.9(a). The $N = 6$ sector has lower energy than $N = 4$ sector. Now we choose $\mu = 0$, $C = 0.2$, then we find that the lowest energy is now in the $N = 4$ sector, see Fig. 4.9(b). The lowest energy state is in the (4, 1) sector because our special choice of Zeeman coupling in z direction (See Fig. 4.8(b)) guarantee that they are more stable than (4, 2) and (4, 0) states. There are other ways to choose $\mu$ and $C$ to make (4, 1) the lowest energy states. We choose this special set because of two reasons. First, the energy scales of $H_{SC}$ and $H_{BX}$ in our simulations are much larger than the chemical potential term and the charging energy terms. Second, the half width of the BCS wave function is of order $\sqrt{N}$ [100] so $N = 2, 4, 6$ sectors all play important roles in the ground state properties. Therefore, change of $\mu$ and $C$ will not affect the topological properties of the system. Experimentally $C$ should be a fixed number of the system and we only need to tune $\mu$.

Now we include the $H_{SC}$ and $H_{BX}$ into our simulations. Our special choice of a localized $H_{BX}$ allow us to focus only on one domain wall. The edge states on the other domain wall will be gaped out due to our spreading superconducting potential. As discussed in Sec.V, we anticipate parafermion modes will appear in the case when both superconducting pairing $\Delta$ and the tunneling $B$ are very large. In our systems, the emergence of the parafermion mode means the appearance of a six fold ground state degeneracy. Exactly diagonalizing our Hamiltonian Eq. (4.33), we obtain the spectrums shown in Fig. 4.10. In Fig. 4.10(a), we fixed the value of B to 10000T and vary the superconducting pairing $\Delta$. We find that the system evolve from unique ground state to a three fold ground state and then to six fold ground state. We argue that this six fold ground state degeneracy represents the emergence of parafermions. They do not have exactly the same energy, because our effective theory is for 1D systems and now we simulate the 2D system. The tunneling between edge states and other bulk orbitals may be effectively regarded as perturbations which will lift the degeneracy. In addition, our simulation is for a small number of particles so the overlap of parafermions will also lift the degeneracy. Anyway, from Fig. 4.10 we

can still identify the ground state sub-space from the excitation space. When we further increased the pairing potential, we see that the system evolve into a three fold degeneracy state. The reason for this may be that the system enters a gapped phase which are dominated by $\Delta$. In Fig. 4.10(b), we fixed the value of $\Delta$ to 50 and vary the B. We also see that the six fold degenerate ground states appear when B is large. But when further increasing the B, it may also enter the three fold degenerate tunneling dominate gapped regime. To summarize, by exact diagonalizing the Hamiltonian, we find that the system can enter a phase which has six-fold degenerate ground states. This six-fold nearly degenerate ground state sub-space is well separated from the excitations by a gap. As it happens at both $\Delta$ and B are large, we argue that they are the parafermion modes according the our analytic analysis in the previous section.

To further analyze the properties of the system, we plot the phase diagram of the system in a wide range of $\Delta$ and B in Fig. 4.11. We find that the phase A, which has six fold ground state degeneracy (represented by red points in Fig. 4.11), are separated from other gapped phases by gapless regimes. When we go from other gapped phases to phase A, the gaps first close and then reopen. A quantum phase transition may occur during this process. Combining with our analytical analysis, we are legitimate to call the phase A as the topological superconducting phase which supports parafermions.

## 4.7 Conclusion

In this chapter, we show that parafermion zero modes can emerge in the spin transitions in the fractional quantum Hall regime. Exact diagonalization of the Hamiltonian in a disk and torus geometries proves the existence of the counter-propagating edge states with different spin polarizations at the boundaries between areas of the electron liquid in spin polarized and unpolarized $\nu = 2/3$ phases. By analytical and numerical methods we find the conditions for parafermion zero modes to emerge when these edge states are coupled to an s-wave superconductors. The phase diagram in-

dicates that the parafermionic phase, which is represented by the six-fold ground state degeneracy, is separated from other phases by a topological phase transition. Parafermion modes in fractional quantum Hall systems coupled to s-wave superconductors are experimentally feasible. They present a vital step toward the realization of Fibonacci anyons that allow a full set of quantum operations with topologically protected quasiparticles.

# REFERENCES

# REFERENCES


[1] Ettore Majorana. Teoria simmetrica dell'elettrone e del positrone. *Il Nuovo Cimento (1924-1942)*, 14(4):171, 1937.

[2] A Yu Kitaev. Unpaired majorana fermions in quantum wires. *Physics-Uspekhi*, 44(10S):131, 2001.

[3] Paul Adrien Maurice Dirac. The quantum theory of the electron. *Proc. R. Soc. Lond. A*, 117(778):610–624, 1928.

[4] Michael E Peskin. *An introduction to quantum field theory*. CRC Press, 2018.

[5] Frank Wilczek. Majorana returns. *Nature Physics*, 5(9):614, 2009.

[6] Palash B Pal. Dirac, majorana, and weyl fermions. *American Journal of Physics*, 79(5):485–498, 2011.

[7] Nicholas Read and Dmitry Green. Paired states of fermions in two dimensions with breaking of parity and time-reversal symmetries and the fractional quantum hall effect. *Physical Review B*, 61(15):10267, 2000.

[8] Gregory Moore and Nicholas Read. Nonabelions in the fractional quantum hall effect. *Nuclear Physics B*, 360(2-3):362–396, 1991.

[9] Chetan Nayak, Steven H Simon, Ady Stern, Michael Freedman, and Sankar Das Sarma. Non-abelian anyons and topological quantum computation. *Reviews of Modern Physics*, 80(3):1083, 2008.

[10] Jason Alicea. New directions in the pursuit of majorana fermions in solid state systems. *Reports on progress in physics*, 75(7):076501, 2012.

[11] Leonid P Rokhinson, Xinyu Liu, and Jacek K Furdyna. The fractional ac josephson effect in a semiconductor–superconductor nanowire as a signature of majorana particles. *Nature Physics*, 8(11):795, 2012.

[12] Jon M Leinaas and Jan Myrheim. On the theory of identical particles. *Il Nuovo Cimento B (1971-1996)*, 37(1):1–23, 1977.

[13] Xiao-Gang Wen. *Quantum field theory of many-body systems: from the origin of sound to an origin of light and electrons*. Oxford University Press on Demand, 2004.

[14] Dmitri A Ivanov. Non-abelian statistics of half-quantum vortices in p-wave superconductors. *Physical review letters*, 86(2):268, 2001.

[15] B Andrei Bernevig and Taylor L Hughes. *Topological insulators and topological superconductors*. Princeton university press, 2013.

[16] Jay D Sau, Roman M Lutchyn, Sumanta Tewari, and S Das Sarma. Generic new platform for topological quantum computation using semiconductor heterostructures. *Physical review letters*, 104(4):040502, 2010.

[17] Jingcheng Liang and Yuli Lyanda-Geller. Charge carrier holes and majorana fermions. *Physical Review B*, 95(20):201404, 2017.

[18] Charles L Kane and Eugene J Mele. Z 2 topological order and the quantum spin hall effect. *Physical review letters*, 95(14):146802, 2005.

[19] Markus König, Steffen Wiedmann, Christoph Brüne, Andreas Roth, Hartmut Buhmann, Laurens W Molenkamp, Xiao-Liang Qi, and Shou-Cheng Zhang. Quantum spin hall insulator state in hgte quantum wells. *Science*, 318(5851):766–770, 2007.

[20] Yuval Oreg, Gil Refael, and Felix von Oppen. Helical liquids and majorana bound states in quantum wires. *Physical review letters*, 105(17):177002, 2010.

[21] Roman M Lutchyn, Jay D Sau, and S Das Sarma. Majorana fermions and a topological phase transition in semiconductor-superconductor heterostructures. *Physical review letters*, 105(7):077001, 2010.

[22] MV Durnev, MM Glazov, and EL Ivchenko. Spin-orbit splitting of valence subbands in semiconductor nanostructures. *Physical Review B*, 89(7):075430, 2014.

[23] GE Simion and YB Lyanda-Geller. Magnetic field spectral crossings of luttinger holes in quantum wells. *Physical Review B*, 90(19):195410, 2014.

[24] Christoph Kloeffel, Mircea Trif, and Daniel Loss. Strong spin-orbit interaction and helical hole states in ge/si nanowires. *Physical Review B*, 84(19):195314, 2011.

[25] Franziska Maier, Jelena Klinovaja, and Daniel Loss. Majorana fermions in ge/si hole nanowires. *Physical Review B*, 90(19):195421, 2014.

[26] D Csontos, Patrik Brusheim, U Zülicke, and HQ Xu. Spin-3 2 physics of semiconductor hole nanowires: Valence-band mixing and tunable interplay between bulk-material and orbital bound-state spin splittings. *Physical Review B*, 79(15):155323, 2009.

[27] A Yu Kitaev. Fault-tolerant quantum computation by anyons. *Annals of Physics*, 303(1):2–30, 2003.

[28] Jason Alicea, Yuval Oreg, Gil Refael, Felix Von Oppen, and Matthew PA Fisher. Non-abelian statistics and topological quantum information processing in 1d wire networks. *Nature Physics*, 7(5):412, 2011.

[29] Y Maeno, H Hashimoto, K Yoshida, S Nishizaki, T Fujita, JG Bednorz, and F Lichtenberg. Superconductivity in a layered perovskite without copper. *Nature*, 372(6506):532, 1994.

[30] Liang Fu and Charles L Kane. Superconducting proximity effect and majorana fermions at the surface of a topological insulator. *Physical review letters*, 100(9):096407, 2008.

[31] Roman M Lutchyn, Tudor D Stanescu, and S Das Sarma. Search for majorana fermions in multiband semiconducting nanowires. *Physical review letters*, 106(12):127001, 2011.

[32] Jason Alicea. Majorana fermions in a tunable semiconductor device. *Physical Review B*, 81(12):125318, 2010.

[33] Jay D Sau, Sumanta Tewari, and S Das Sarma. Experimental and materials considerations for the topological superconducting state in electron-and hole-doped semiconductors: Searching for non-abelian majorana modes in 1d nanowires and 2d heterostructures. *Physical Review B*, 85(6):064512, 2012.

[34] Li Mao, Ming Gong, E Dumitrescu, Sumanta Tewari, and Chuanwei Zhang. Hole-doped semiconductor nanowire on top of an s-wave superconductor: a new and experimentally accessible system for majorana fermions. *Physical review letters*, 108(17):177001, 2012.

[35] Daniel P Arovas and Yuli Lyanda-Geller. Non-abelian geometric phases and conductance of spin-3 2 holes. *Physical Review B*, 57(19):12302, 1998.

[36] YB Lyanda-Geller, TL Reinecke, and M Bayer. Exciton fine structure in coupled quantum dots. *Physical Review B*, 69(16):161308, 2004.

[37] Denis V Bulaev and Daniel Loss. Spin relaxation and decoherence of holes in quantum dots. *Physical review letters*, 95(7):076805, 2005.

[38] B Andrei Bernevig and Shou-Cheng Zhang. Intrinsic spin hall effect in the two-dimensional hole gas. *Physical review letters*, 95(1):016801, 2005.

[39] CHL Quay, TL Hughes, JA Sulpizio, LN Pfeiffer, KW Baldwin, KW West, D Goldhaber-Gordon, and R De Picciotto. Observation of a one-dimensional spin–orbit gap in a quantum wire. *Nature Physics*, 6(5):336, 2010.

[40] SS Nedorezov. Space quantization in semiconductor films. *SOV PHYS SOLID STATE*, 12(8):1814–1819, 1971.

[41] NA Merkulov, VI Perel, and ME Portnoi. Momentum alignment and spin orientation of photoexcited electrons in quantum wells. 1991.

[42] EI Rashba and E Ya Sherman. Spin-orbital band splitting in symmetric quantum wells. *Physics Letters A*, 129(3):175–179, 1988.

[43] Yuli Lyanda-Geller. Pure spin decoherence in quantum dots. *arXiv preprint arXiv:1210.7825*, 2012.

[44] Roland Winkler. *Spin-orbit coupling effects in two-dimensional electron and hole systems*, volume 191. Springer Science & Business Media, 2003.

[45] Lok C Lew Yan Voon and Morten Willatzen. *The kp method: electronic properties of semiconductors*. Springer Science & Business Media, 2009.

[46] Peter Y Yu and Manuel Cardona. *Fundamentals of semiconductors: physics and materials properties*. Springer, 1996.

[47] G Pikus. G. pikus, v. marushchak, and a. titkov, fiz. tekh. poluprovodn. 22, 185 (1988). *Fiz. Tekh. Poluprovodn.*, 22:185, 1988.

[48] W Knap, C Skierbiszewski, A Zduniak, E Litwin-Staszewska, D Bertho, F Kobbi, JL Robert, GE Pikus, FG Pikus, SV Iordanskii, et al. Weak antilocalization and spin precession in quantum wells. *Physical Review B*, 53(7):3912, 1996.

[49] SV Iordanskii, Yu B Lyanda-Geller, and GE Pikus. Weak localization in quantum wells with spin-orbit interaction. *ZhETF Pisma Redaktsiiu*, 60:199, 1994.

[50] R Winkler, H Noh, E Tutuc, and M Shayegan. Anomalous rashba spin splitting in two-dimensional hole systems. *Physical Review B*, 65(15):155303, 2002.

[51] LP Rokhinson, LN Pfeiffer, and KW West. Spontaneous spin polarization in quantum point contacts. *Physical review letters*, 96(15):156602, 2006.

[52] R Danneau, O Klochan, WR Clarke, LH Ho, AP Micolich, MY Simmons, AR Hamilton, M Pepper, DA Ritchie, and U Zülicke. Zeeman splitting in ballistic hole quantum wires. *Physical review letters*, 97(2):026403, 2006.

[53] Jay D Sau, Sumanta Tewari, Roman M Lutchyn, Tudor D Stanescu, and S Das Sarma. Non-abelian quantum order in spin-orbit-coupled semiconductors: Search for topological majorana particles in solid-state systems. *Physical Review B*, 82(21):214509, 2010.

[54] Tudor D Stanescu, Roman M Lutchyn, and S Das Sarma. Majorana fermions in semiconductor nanowires. *Physical Review B*, 84(14):144522, 2011.

[55] Vincent Mourik, Kun Zuo, Sergey M Frolov, SR Plissard, Erik PAM Bakkers, and Leo P Kouwenhoven. Signatures of majorana fermions in hybrid superconductor-semiconductor nanowire devices. *Science*, 336(6084):1003–1007, 2012.

[56] Jie Xiang, Andy Vidan, Michael Tinkham, Robert M Westervelt, and Charles M Lieber. Ge/si nanowire mesoscopic josephson junctions. *Nature nanotechnology*, 1(3):208, 2006.

[57] Vlad S Pribiag, Arjan JA Beukman, Fanming Qu, Maja C Cassidy, Christophe Charpentier, Werner Wegscheider, and Leo P Kouwenhoven. Edge-mode superconductivity in a two-dimensional topological insulator. *Nature nanotechnology*, 10(7):593, 2015.

[58] Andrew Patrick Higginbotham, Sven Marian Albrecht, G Kiršanskas, Willy Chang, Ferdinand Kuemmeth, Peter Krogstrup, Thomas Sand Jespersen, Jesper Nygård, Karsten Flensberg, and Charles M Marcus. Parity lifetime of bound states in a proximitized semiconductor nanowire. *Nature Physics*, 11(12):1017, 2015.

[59] Sean Hart, Hechen Ren, Timo Wagner, Philipp Leubner, Mathias Mühlbauer, Christoph Brüne, Hartmut Buhmann, Laurens W Molenkamp, and Amir Yacoby. Induced superconductivity in the quantum spin hall edge. *Nature Physics*, 10(9):638, 2014.

[60] RP Panguluri, KC Ku, T Wojtowicz, X Liu, JK Furdyna, YB Lyanda-Geller, N Samarth, and B Nadgorny. Andreev reflection and pair-breaking effects at the superconductor/magnetic semiconductor interface. *Physical Review B*, 72(5):054510, 2005.

[61] Stefan Rex and Asle Sudbø. Tilting of the magnetic field in majorana nanowires: critical angle and zero-energy differential conductance. *Physical Review B*, 90(11):115429, 2014.

[62] CK Gaspe, M Edirisooriya, TD Mishima, PAR Dilhani Jayathilaka, RE Doezema, SQ Murphy, MB Santos, LC Tung, and Y-J Wang. Effect of strain and confinement on the effective mass of holes in insb quantum wells. *Journal of Vacuum Science & Technology B, Nanotechnology and Microelectronics: Materials, Processing, Measurement, and Phenomena*, 29(3):03C110, 2011.

[63] Michael H Freedman, Michael J Larsen, and Zhenghan Wang. The two-eigenvalue problem and density of jones representation of braid groups. *Communications in mathematical physics*, 228(1):177–199, 2002.

[64] David J Clarke, Jason Alicea, and Kirill Shtengel. Exotic non-abelian anyons from conventional fractional quantum hall states. *Nature communications*, 4:1348, 2013.

[65] Adrian Hutter and Daniel Loss. Quantum computing with parafermions. *Physical Review B*, 93(12):125105, 2016.

[66] Roger SK Mong, David J Clarke, Jason Alicea, Netanel H Lindner, Paul Fendley, Chetan Nayak, Yuval Oreg, Ady Stern, Erez Berg, Kirill Shtengel, et al. Universal topological quantum computation from a superconductor-abelian quantum hall heterostructure. *Physical Review X*, 4(1):011036, 2014.

[67] Daniel Arovas, John R Schrieffer, and Frank Wilczek. Fractional statistics and the quantum hall effect. In *Selected Papers Of J Robert Schrieffer: In Celebration of His 70th Birthday*, pages 270–271. World Scientific, 2002.

[68] Parsa Bonderson and JK Slingerland. Fractional quantum hall hierarchy and the second landau level. *Physical Review B*, 78(12):125323, 2008.

[69] Jae-Seung Jeong, Hantao Lu, Ki Hoon Lee, Kenji Hashimoto, Suk Bum Chung, and Kwon Park. Competing states for the fractional quantum hall effect in the 1/3-filled second landau level. *Physical Review B*, 96(12):125148, 2017.

[70] K v Klitzing, Gerhard Dorda, and Michael Pepper. New method for high-accuracy determination of the fine-structure constant based on quantized hall resistance. *Physical Review Letters*, 45(6):494, 1980.

[71] Jainendra K Jain. *Composite fermions*. Cambridge University Press, 2007.

[72] Gabriele Giuliani and Giovanni Vignale. *Quantum theory of the electron liquid*. Cambridge university press, 2005.

[73] Daniel C Tsui, Horst L Stormer, and Arthur C Gossard. Two-dimensional magnetotransport in the extreme quantum limit. *Physical Review Letters*, 48(22):1559, 1982.

[74] Robert B Laughlin. Anomalous quantum hall effect: an incompressible quantum fluid with fractionally charged excitations. *Physical Review Letters*, 50(18):1395, 1983.

[75] Xiao-Gang Wen. Theory of the edge states in fractional quantum hall effects. *International Journal of Modern Physics B*, 6(10):1711–1762, 1992.

[76] Xiao-Gang Wen. Topological orders and edge excitations in fractional quantum hall states. *Advances in Physics*, 44(5):405–473, 1995.

[77] AH MacDonald. Edge states in the fractional-quantum-hall-effect regime. *Physical review letters*, 64(2):220, 1990.

[78] C de C Chamon and XG Wen. Sharp and smooth boundaries of quantum hall liquids. *Physical Review B*, 49(12):8227, 1994.

[79] Xin Wan, Kun Yang, and EH Rezayi. Reconstruction of fractional quantum hall edges. *Physical review letters*, 88(5):056802, 2002.

[80] Jianhui Wang, Yigal Meir, and Yuval Gefen. Edge reconstruction in the $\nu = 2/3$ fractional quantum hall state. *Physical review letters*, 111(24):246803, 2013.

[81] Ying-Hai Wu, GJ Sreejith, and Jainendra K Jain. Microscopic study of edge excitations of spin-polarized and spin-unpolarized $\nu = 2/3$ fractional quantum hall effect. *Physical Review B*, 86(11):115127, 2012.

[82] Xiao-Gang Wen. Chiral luttinger liquid and the edge excitations in the fractional quantum hall states. *Physical Review B*, 41(18):12838, 1990.

[83] Paul Fendley. Parafermionic edge zero modes in zn-invariant spin chains. *Journal of Statistical Mechanics: Theory and Experiment*, 2012(11):P11020, 2012.

[84] Tailung Wu, Zhong Wan, Aleksandr Kazakov, Ying Wang, George Simion, Jingcheng Liang, Kenneth W West, Kirk Baldwin, Loren N Pfeiffer, Yuli Lyanda-Geller, et al. Formation of helical domain walls in the fractional quantum hall regime as a step toward realization of high-order non-abelian excitations. *Physical Review B*, 97(24):245304, 2018.

[85] M Baraban, NE Bonesteel, and SH Simon. Resources required for topological quantum factoring. *Physical Review A*, 81(6):062317, 2010.

[86] Jason Alicea and Paul Fendley. Topological phases with parafermions: theory and blueprints. *Annual Review of Condensed Matter Physics*, 7:119–139, 2016.

[87] JP Eisenstein, HL Stormer, LN Pfeiffer, and KW West. Evidence for a spin transition in the $\nu = 2/3$ fractional quantum hall effect. *Physical Review B*, 41(11):7910, 1990.

[88] JH Smet, RA Deutschmann, Werner Wegscheider, Gerhard Abstreiter, and K von Klitzing. Ising ferromagnetism and domain morphology in the fractional quantum hall regime. *Physical review letters*, 86(11):2412, 2001.

[89] Aleksandr Kazakov, George Simion, Yuli Lyanda-Geller, Valery Kolkovsky, Zbigniew Adamus, Grzegorz Karczewski, Tomasz Wojtowicz, and Leonid P Rokhinson. Mesoscopic transport in electrostatically defined spin-full channels in quantum hall ferromagnets. *Physical review letters*, 119(4):046803, 2017.

[90] GE Simion, A Kazakov, LP Rokhinson, T Wojtowicz, and YB Lyanda-Geller. Disorder-generated non-abelions. *arXiv preprint arXiv:1707.02929*, 2017.

[91] CWJ Beenakker. Edge channels for the fractional quantum hall effect. *Physical review letters*, 64(2):216, 1990.

[92] Dmitri B Chklovskii. Structure of fractional edge states: A composite-fermion approach. *Physical Review B*, 51(15):9895, 1995.

[93] Xiao-Gang Wen and Anthony Zee. Topological structures, universality classes, and statistics screening in the anyon superfluid. *Physical Review B*, 44(1):274, 1991.

[94] IA McDonald and FDM Haldane. Topological phase transition in the $\nu = 2/3$ quantum hall effect. *Physical Review B*, 53(23):15845, 1996.

[95] JE Moore and FDM Haldane. Edge excitations of the $\nu =$ spin-singlet quantum hall state. *Physical Review B*, 55(12):7818, 1997.

[96] Tailung Wu, Aleksandr Kazakov, George Simion, Zhong Wan, Jingcheng Liang, Kenneth W West, Kirk Baldwin, Loren N Pfeiffer, Yuli Lyanda-Geller, and Leonid P Rokhinson. Parafermion supporting platform based on spin transitions in the fractional quantum hall effect regime. *arXiv preprint arXiv:1709.07928*, 2017.

[97] D Yoshioka, BI Halperin, and PA Lee. Ground state of two-dimensional electrons in strong magnetic fields and 1 3 quantized hall effect. *Physical review letters*, 50(16):1219, 1983.

[98] Xiao-Gang Wen and Qian Niu. Ground-state degeneracy of the fractional quantum hall states in the presence of a random potential and on high-genus riemann surfaces. *Physical Review B*, 41(13):9377, 1990.

[99] Cécile Repellin, Ashley M Cook, Titus Neupert, and Nicolas Regnault. Numerical investigation of gapped edge states in fractional quantum hall-superconductor heterostructures. *npj Quantum Materials*, 3(1):14, 2018.

[100] Pierre-Gilles De Gennes. *Superconductivity of metals and alloys*. CRC Press, 2018.

VITA

# VITA

**Education**

• Ph.D. Department of Physics and Astronomy, Purdue University, 08/2012~12/2018.

• B.S. School of the Gifted Young, University of Science and Technology of China, 09/2008~07/2012.

**Interests**

• Quantum computation and quantum information, Exotic phases of matter, Fractional quantum Hall effect, High $T_c$ superconductivity, Quantum entanglement, Exactly solvable models

• History, Painting

**Publication**

• **Jingcheng Liang**, George Simion and Yuli Lyanda-Geller, "Parafermions in the Fractional Quantum Hall Effect Spin Transition". To be submitted.

• Tailung Wu, Zhong Wan, Aleksandr Kazakov, Ying Wang, George Simion, **Jingcheng Liang**, Kenneth W. West, Kirk Baldwin, Loren N. Pfeiffer, Yuli Lyanda-Geller, Leonid P. Rokhinson, "Formation of helical domain walls in the fractional quantum Hall regime as a step toward realization of high-order non-Abelian excitations". Phys. Rev. B 97, 245304 (2018).

• **Jingcheng Liang** and Yuli Lyanda-Geller, "Charge carrier holes and Majorana fermions". Phys. Rev. B 95, 201404 (2017).

• J. J. Ying, **J. C. Liang**, X. G. Luo, Y. J. Yan, A. F. Wang, P. Cheng, G. J. Ye, J. Q. Ma and X. H. Chen, "The magnetic phase diagram of $Ca_{1x}Sr_xCo_2As_2$ single crystals". EPL (Europhysics Letters) 104(6), 67005 (2014).

• J. J. Ying, **J. C. Liang**, X. G. Luo, X. F. Wang, Y. J. Yan, M. Zhang, A. F. Wang,

Z. J. Xiang, G. J. Ye, P. Cheng, and X. H. Chen, "Transport and magnetic properties of La-doped $CaFe_2As_2$". Phys. Rev. B 85, 144514 (2012).

**Awards**

- (2018) Edward S. Akeley Award, Purdue University.
- (2018) DCMP Graduate Student Travel Award of APS.
- (2012 - 2014) Frederick N. Andrews Fellowship, Purdue University.
- (2012) Ranked the first in the qualifying exam (Physics, Purdue).
- (2012) Excellent Undergraduate Thesis of USTC.
- (2009 - 2011) Outstanding Student Scholarship (Grade 2).
- (2007) First Prize of Chinese Physics Olympiad.